

**Complete characterization of sink-strengths for 1D to 3D  
mobilities of defect clusters.**

**II. Bridging between limiting cases with effective sink-strengths  
calculations.**

Gilles Adjanor\*

*EDF Lab, Les Renardières, Materials and Mechanics  
of Components Departement, Moret-sur-Loing France*

(Dated: July 23, 2020)

## Abstract

In a companion paper, we proposed new analytical expressions of cluster sink-strengths (CSS) indispensable to any complete parameterization of rate equations cluster dynamics accounting for reaction between defect clusters populations having a 1D-mobility. Indeed, simulating more than seconds of microstructure evolution in systems fast diffusing species such as self-interstitial atom (SIA) clusters relies on establishing the CSS for Rate-equation cluster dynamics which critical depends on the complex mobilities of clusters. In this second paper, we estimate effective CSS by Kinetic Monte-Carlo on wide ranges of radii, rotation energies, diffusion coefficients and concentrations of both reaction partners. Symmetric roles of some parameters are used to infer a generic form for a semi-analytical expression of CSS depending on all these interaction parameters: it is composed of, on one hand, the various analytical expressions established for the limiting cases and, on the other hand, of fitted transition functions that allow a gradual switching between them. The analysis of the residuals shows that the overall agreement is reasonably good: it is only in the transition zones that discrepancies are located. This semi-analytical expression answers our a practical need for CSS evaluation in our typical range of conditions, but further extending this range to much smaller diffusion coefficients ratios, it is quite striking to see that the domain for 1D-1D mobility is very extended: for a  $10^{-3}$  ratio the computed CSS is still not correctly described by the 1D-CSS with respect to a fixed sink (1D-0), but rather by the established 1D-1D expression. For our typical sets of conditions, it is only when approaching a ratio of  $10^{-6}$  that the 1D-0 CSS starts to become more relevant. This highlights the counter-intuitive fact that the growth kinetics of moderately trapped 1D mobile loops although described by a reduced effective mobility may not be described by 1D-0 kinetics but rather by appropriately corrected 1D-1D CSS which have completely different order of magnitude and kinetic orders.

**Usage:** Companion paper: [1]

**PACS numbers:** 05.40.Fb, 05.10.Ln, 36.40.Sx, 61.72.J-, 61.80.Az, 66.30.Lw, 82.40.Ck

**Keywords:** Diffusion, Rate equation cluster dynamics, Sink strengths, Dislocation loops mobility

---

\* gilles.adjani@edf.fr

## I. INTRODUCTION

Following the goal of establishing a complete parameterization of cluster sink-strengths (CSS) for any type of clusters mobilities including both species mixed mobilities (i.e. rotations of glide directions, noted  $1DR - 1DR$ ), we have established in a companion paper [1] analytical expressions for  $1D - 1D$  absorption including the diffusion anisotropy analog case (diffusion coefficient ratio being different than one). This task is essential to a rate-equation cluster dynamics (RECD) modeling of microstructure evolution of defect clusters populations according to the state of knowledge on loops mobilities, which are of primary importance regarding material properties evolutions in both fission and fusion reactors, but also nucleation and growth processes at thermal equilibrium.

In section II, the effective CSS are estimated by OKMC for the most general case of  $1DR - 1DR$  CSS with finite rotation energies. Estimates from simulation are required because no general analytical formula is at hand. This is done for a very large set of conditions in terms of D-ratio ( $\mathcal{D} = D_B/D_A$ ) and of rotation energies  $E_A$ ,  $E_B$  couples. The evolution of CSS with these three parameters is then rationalized by proposing a semi-analytical formula, matching the analytical formulas for the limiting cases of  $3D_A - 3D_B$ ,  $1D_A - 3D_B$  and  $1D_A - 1D_B$  CSS and fitting the transition between them thanks to a combination of sigmoid-type functions. The fit is made on one couple of concentrations ( $C_A, C_B$ ), and reproduces with similar levels of accuracy other couples of concentrations, thus assessing for the broad validity of this semi-analytical formula. Given its good ability to reproduce the effective CSS over the many orders of magnitude over which they evolve, the agreement can be considered as very reasonable. The interpretation of the CSS evolution heavily relies on the D-ratio exponents: as highlighted on limiting cases when the D-ratio varies, the CSS mostly varies like  $(D_A/D_B)^\delta$ , the exponent being characteristic of types of the mobilities. A map of effective  $\delta$  values helps the interpretations and the precision of semi-analytical formula heavily relies on its main trends. On this map, domains of different mobility dimensionality clearly appear, and their characteristic exponents are connected with the limiting cases for  $1D_A - 1D_B$  and  $1D_A - 3D_B$  anisotropic analog of the CSS ( $(D_A \neq D_B)$ ). But in the limited range of D-ratios investigated for the purpose of high precision fitting, these domains do not close: even for quite large D-ratios, the fixed sink limit is not reached. At section II B, we investigate the closure of these domains, i.e. the convergence of effective

CSS towards the analytical CSS with respect to a fixed sink when the D-ratio gets lower ( $\Delta = \log_{10}(D_A/D_B)$  higher). As we shall see, it is only when reaching much smaller D-ratios than for our typical set of conditions that the slowest specie can be considered as immobile regarding CSS expressions. As discussed at section IV and validated at section III by comparing RECD to extensive OKMC simulation of complete microstructure evolutions, this implies a quite broad relevance of the established general CSS expression, even when the effective mobilities of species are considerably lowered after trapping by impurities or elastic fields. A more general consequence of this, the prevalence of aggregation (termed here as growth by mutual mobility) over Ostwald ripening is also discussed.

## II. METHOD AND RESULTS

When dealing with 1D mobilities, the convergence of CSS estimates is known to be very slow [2]. In the Annex A, we detail the OKMC simulation procedure for such adequate calculation, and we also show in the Annex B that the conditions for the true convergence of object kinetic Monte-Carlo (OKMC) CSS estimates are the extremely delicate and demanding. Nevertheless, thanks to validated simple models, the conditions for estimates convergence can be established using three criteria: the first criterion states that lowest number species ( $\text{Min}(N_A, N_B)$ ) should be greater than the smallest box dimension in unit cells, the second criterion states that the number of reactions to be performed should be at least equal to the total number of species  $N_A + N_B$  and the last criterion is that a few tens of CSS estimates should be used to assess their standard deviations to mean ratio.

In the calculations presented in the rest of this article, the three preceding convergence criteria are met, so the computed CSS are now referred as “effective CSS”  $\kappa_{\text{eff}}^2$  instead of estimates of the CSS.

First, we present results for the  $C_A = C_B$  for a few  $(E_A, E_B)$  combinations, in order to establish trends.

Figure 1 presents effective CSS computed from simulation with  $(E_A = 2 \text{ eV}, E_B = 2 \text{ eV})$  at various concentrations. With both rotation energies as high as 2 eV at 573 K, the particles will have a very large mean-free path before rotation compared to box size, so they can safely be treated as purely 1D-mobile and thus comparison with the analytical  $\kappa_{1D-1D}^2$  is relevant. For each  $R$  value, the linear relation between  $\Delta = \log_{10}(D_A/D_B)$  and  $\log_{10}(\kappa_{\text{eff}}^2)$

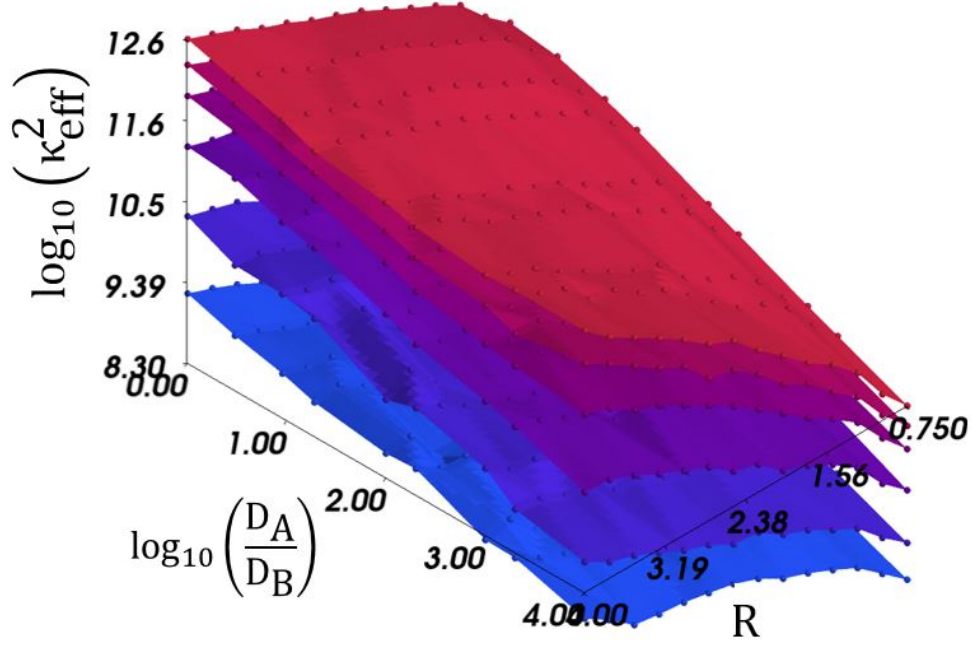


Figure 1. Logarithm of the effective CSS  $\kappa_{\text{eff}}^2$  in  $\text{cm}^{-2}$  as a function of the radius and of  $\Delta = \log_{10}(D_A/D_B)$  for the conditions  $(E_A = 2, E_B = 2)$  (eV) and  $C_A = C_B$  ranging from  $3.4 \times 10^{16}, 6.8 \times 10^{16}, 1.7 \times 10^{17}, 3.4 \times 10^{17}, 5.1 \times 10^{17}, 6.8 \times 10^{17} \text{ cm}^{-3}$  (from blue to red surfaces).

on the figure indeed suggests a power-law dependency of the CSS on the D-ratio. Detailed analysis indeed shows that it follows the expected characteristic exponent  $-1/3$  excepted from the diffusion anisotropy analogy highlighted in the companion paper.

The evolution of CSS surfaces with  $R$  are clearly more complex, and changing the representation to  $\log_{10}(R)$  would not reveal a simple and general scaling. Again, this is not surprising, as according to Eq. B7, the CSS should depend on  $R$  through  $\overline{R_{\text{eff}}}$  and the inverse logarithm of  $R^3$ .

From the preceding part, we can conclude that the proposed analytical expression match well the computed effective CSS for the  $1D-1D$  case. Other limiting cases like  $1D-3D$  and  $3D-3D$  (rotation energy couples set to  $(E_A = 0 \text{ eV}, E_B = 2 \text{ eV})$  and  $(E_A = 0 \text{ eV}, E_B = 0 \text{ eV})$  respectively) were checked to follow their related limiting case CSS expressions, although for the sake of conciseness their corresponding graphs are not shown here. However, this approach reaches its limits when dealing with intermediate values of rotation energies which do not correspond to a well defined limiting case: with a direct plot of a set of CSS surfaces

depending on D-ratio and  $R$ , it can be difficult to determine which CSS analytical expression is the best match. Moreover, pursuing the approach of estimating CSS for many different couples of concentrations, there might be few hope of rationalizing the results: concentrations relevant to typical irradiation or nucleation conditions span over too much order of magnitudes.

We will thus adopt a different approach in the next sections.

### A. Semi-analytical expression for general sink-strengths

We will now focus on establishing a semi-analytical expression of CSS for the general case of  $(E_A, E_B) \in [0, 2] \times [0, 2]$  (eV). and reproducing the identified analytical expressions for limiting cases. The functions allowing for the transition between the limiting cases will be fitted on simulation results which makes the approach not fully analytical but only semi-analytical. For the purpose of this fitting procedure, a first set of 1728 conditions has been simulated. It corresponds to the following parameters ranges:

$$\begin{aligned}
C_A &= C_B = 1 \times 10^{17} \text{cm}^{-3}, \\
R_A &= R_B = 0.5 \text{ nm}, \\
(E_A, E_B) &\in \{0, 0.1, 0.2, 0.3, 0.4, 0.5, 0.6, 0.7, 0.8, 0.9, 1.0, 2.0\}^2 (\text{eV}). \\
D_A + D_B &= 3.12 \times 10^{-5} \text{cm}^2 \text{s}^{-1}, \\
\Delta = -\log_{10}(\mathcal{D}) &\in \{0, 0.27, 0.54, 0.81, 1.09, 1.36, 1.63, 1.90, 2.18, 2.45, 2.72, 3\}.
\end{aligned} \tag{1}$$

Note that these parameters have been chosen with some guidance from the parameterization in table II from the Annex, but that this choice does not impact the generality of the results to come, thanks their semi-analytic character. One advantage on having the condition  $C_A = C_B$  fixed to a not too low density is that it eases the search for the optimal simulation parameters (such as internal variables for OKMC’s “link-cell” type neighbor finding algorithm, box size, single run duration etc.) valid for the whole set of conditions. Thus, we could obtain coefficients of variation  $\sigma(\kappa_{est}^2)/(\overline{\kappa_{est}^2})$  of 1% on average over all the 1728 conditions and about 5% in the worse cases. The average number of estimates (runs with different initial placements of defects) is equal to ten.

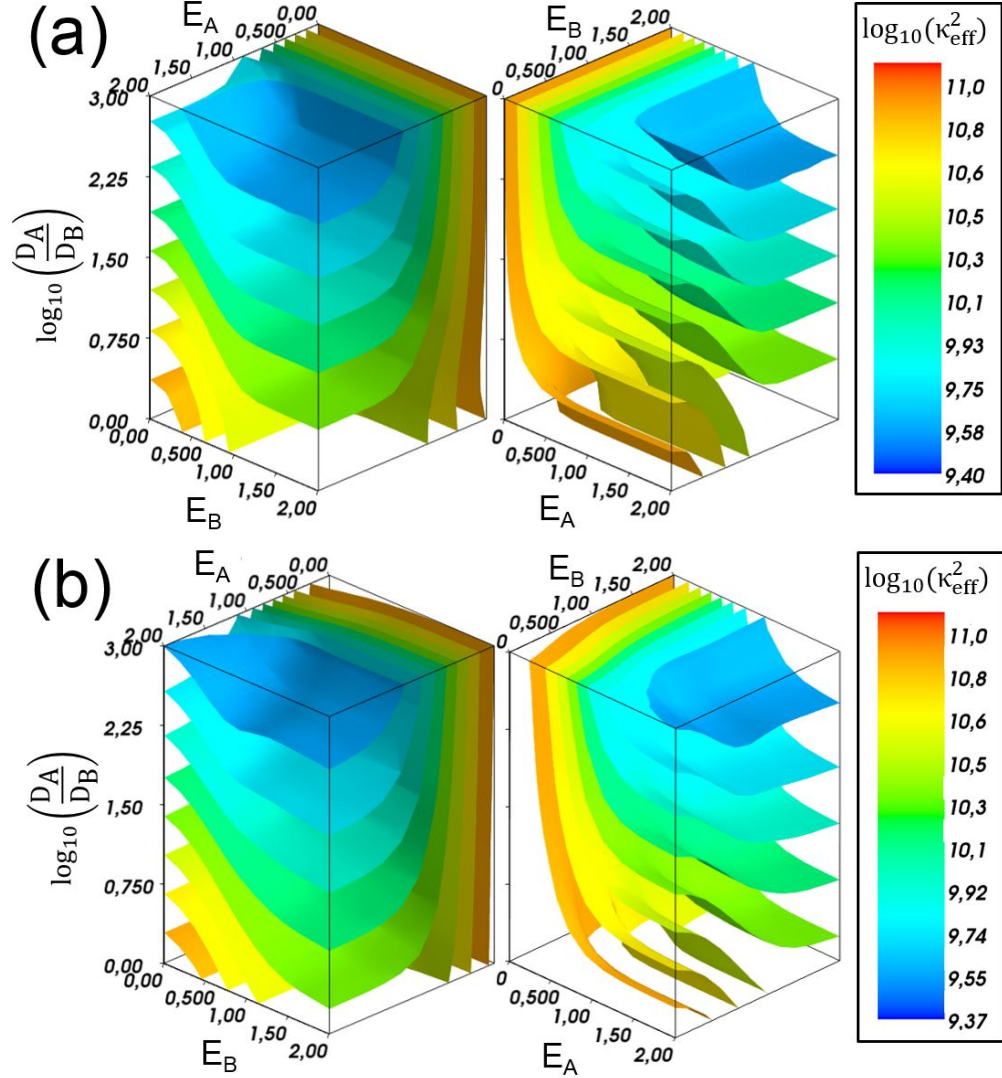


Figure 2. (a) two rotated views of the same  $\log_{10}(\kappa_{\text{eff}}^2)$  (the CSS being in  $\text{cm}^{-2}$ ) isosurfaces in the  $(E_A, E_B, \Delta = \log_{10}(D_A/D_B))$  space. (b) same views of isosurfaces obtained from the semi-analytical formula Eq. 16.

The results are shown on the top panel of Fig. 2. They are displayed in the form of CSS-isosurfaces (represented using the Mayavi library [16]). The overall shape is quite complex but we can nevertheless draw some trends. First we see that for values of A species' rotation energy  $E_A$  close to zero, the CSS reaches the highest values. This is also quite independent of both  $E_B$  and the diffusion coefficients ratio: the corresponding isosurfaces are almost flat and parallel to the  $E_A = 0$  plane. This is because when  $D_A$  is greater  $D_B$ , if  $A$  is purely or almost purely 3D-mobile, the type of mobility of  $B$  has very little influence on absorption

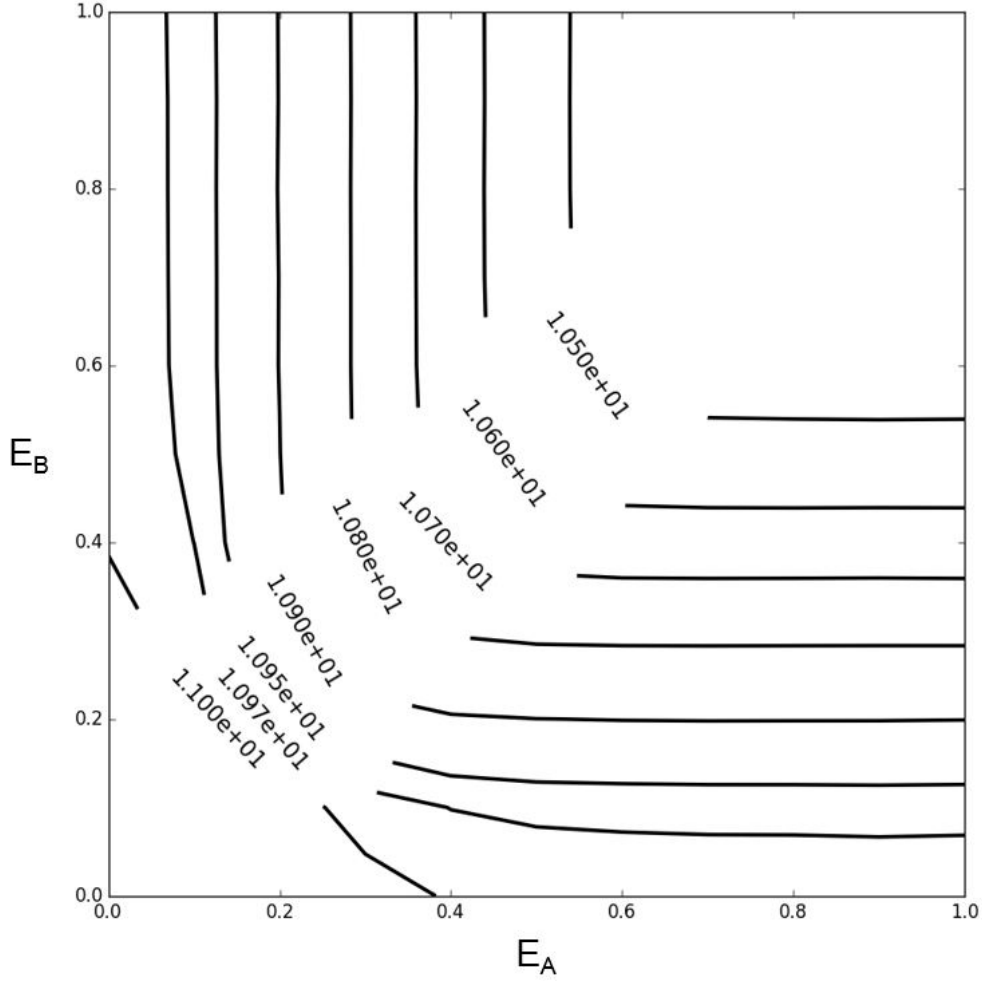


Figure 3. Contours of the decimal logarithm of effective CSS in  $\text{cm}^{-3}$  for  $D_A = D_B$  in the  $(E_A, E_B)$  plane.

probability, the overwhelming efficiency of 3D-mobility will completely dominate. Another case is when  $D_B$  is equal or very close to  $D_A$ ,  $E_A$  and  $E_B$  should play symmetric roles for the CSS. This is indeed what is observed in the Fig. 3. The hyperbolic-like shape of the contour lines can be simply interpreted by the fact that because  $D_A = D_B$ , for  $E_A$  fixed, the CSS depend very weakly on  $E_B$ , so iso-CSS lines should be parallel to  $E_B$  (and conversely for  $E_B$  fixed). Also, we note that globally, whatever the couple  $(E_A, E_B)$  values the CSS varies quite weakly in this isotropic diffusion analog case  $D_A = D_B$ . Nevertheless, it will be important to reproduce these hyperbolic-like shapes, because by extrusion and non-uniform shear along the  $z$ -axis they generate the complex isosurfaces of Fig. 2.

Another salient feature of Fig. 2 is that a series of isosurfaces parts are almost identical



up to a constant translation along the  $z$ -axis. This is particularly striking for large values of  $E_A$ . In this logarithmic representation, the constant spacing along  $\Delta$  between isosurfaces is the signature of the power-law dependencies highlighted in the limiting cases. This clearly holds for specific parts of the  $(E_A, E_B, \Delta)$ -parameter space: the plateau values reached by the surfaces notably when both  $E_A$  and  $E_B$  are large suggest a quite wide range of validity of limiting case analytical formulas. Between these plateau regions there are very clear transition zones where isosurfaces have sigmoid shapes.

All these observations will now guide us to build a semi-analytical CSS expression for any couple of rotation energies, whose transition coefficients will be adjusted on the present data set. Hereafter, we will use the well known “sigmoid” function (also known as the logistic function):

$$\sigma(\lambda, \varepsilon, x) = \frac{1}{1 + \exp[-\lambda(x - \varepsilon)]}. \quad (2)$$

As sketched on Fig. 4, when  $D_A = D_B$ , one very general formulation of the CSS may be:

$$\begin{aligned} \kappa^2(E_A, E_B, D_A, D_A) = & \\ f(E_A) & \left( (1 - g(E_B)) \kappa_{1D-3D}^2 + g(E_B) \kappa_{1D-1D}^2 \right) \\ + (1 - f'(E_A)) & \\ \times \left( (1 - g'(E_B)) \kappa_{3D-3D}^2 + g'(E_B) \kappa_{3D-1D}^2 \right) & \end{aligned}$$

with the functions  $f$ ,  $f'$ ,  $g$  and  $g'$  having the constraints:  $f(0) = f'(0) = g(0) = g'(0) = 0$  and  $f(1) = f'(1) = g(1) = g'(1) = 1$  so that the four limiting cases are recovered:

$$\begin{aligned} \kappa^2(0, 0, D_A, D_A) &= \kappa_{3D-3D}^2(D_A, D_A) \\ \kappa^2(0, \infty, D_A, D_A) &= \kappa_{3D-1D}^2(D_A, D_A) \\ \kappa^2(\infty, 0, D_A, D_A) &= \kappa_{1D-3D}^2(D_A, D_A) \\ \kappa^2(\infty, \infty, D_A, D_A) &= \kappa_{1D-1D}^2(D_A, D_A) \end{aligned}$$

If we impose that  $E_A$  and  $E_B$  play symmetric roles ( $\kappa^2(E_A, E_B, D_A, D_A) = \kappa^2(E_B, E_A, D_A, D_A)$ ) and use  $\kappa_{3D-1D}^2(D_A, D_A) = \kappa_{1D-3D}^2(D_A, D_A)$ , then we must have  $f = g$  and  $f' = g'$  and we

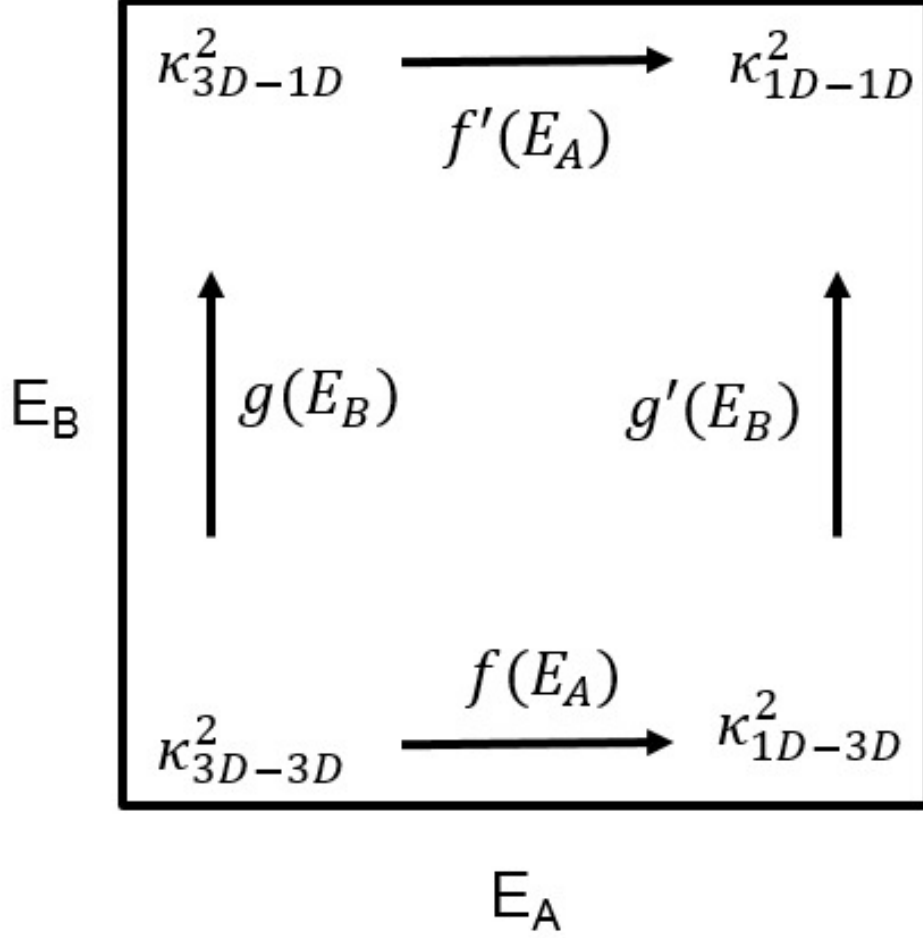


Figure 4. Schematic view of the relation between the fitting function  $f$ ,  $f'$ ,  $g$  and  $g'$  and the limiting cases for the CSS when  $D_A = D_B$  in the  $(E_A, E_B)$  plane.

can cast the CSS to the following form:

$$\begin{aligned} \kappa^2(E_A, E_B, D_A, D_A) = & f(E_A) \left( (1 - f(E_B)) \kappa_{1D-3D}^2 + f(E_B) \kappa_{1D-1D}^2 \right) \\ & + (1 - f'(E_A)) \left( (1 - f'(E_B)) \kappa_{3D-3D}^2 + f'(E_B) \kappa_{1D-3D}^2 \right) \end{aligned} \quad (3)$$

In practice, experimenting various fitting possibilities, it turns out that we can make this form even simpler taking:

$$f'(x) = f(x) = \sigma(\lambda_f, \varepsilon_f, x) \quad (4)$$

$$(5)$$

and a simple fitting procedure leads to  $\lambda_f = 8$  and  $\varepsilon_f = 0.2$ , with overall 5% discrepancy with the simulated data set and a maximum deviation of about 15% for the worse point.

Following the previous findings, we will now assume that the fit can be extended to  $D_A > D_B$  scaling it with the ratio of diffusion coefficients to a power that depends of the dimensionality of the mobilities:

$$\kappa^2(E_A, E_B, D_A, D_B) = \kappa^2(E_A, E_B, D_A, D_A) \quad (6)$$

$$\times \left( \frac{D_A}{D_B} \right)^{\delta(E_A, E_B)} \quad (7)$$

We are now left with the task of defining the exponent function  $\delta$ . The values of delta that should be matched according to the analog limiting cases are sketched on Fig. 5:

- $(E_A = 0, E_B = 0)$  (eV) corresponds to  $3D - 3D$  absorption rates which simply depend on  $(D_A + D_B)$ , that makes  $(1 + (D_A/D_B)^{-1})$  when factoring for  $D_B$  the CSS, which is close to  $1 = (D_A/D_B)^0$  when  $D_A \gg D_B$  in other words a close to zero  $\delta$  value,
- $(E_A = 2, E_B = 2)$  corresponds to  $1D - 1D$  absorption rates with a characteristic exponent of  $-1/3$ , consistently with the related limiting case [1],
- $(E_A = 2, E_B = 0)$  similarly corresponds to  $1D - 3D$  with  $D_A > D_B$  absorption rates leading to a  $-1/2$  exponent [1]

One very simple choice for an exponent function  $\delta$  meeting these requirements is:

$$\delta(E_A, E_B) = \sigma(\varepsilon, \lambda, E_A) \left( -\frac{1}{2} + \frac{1}{6} \sigma(\varepsilon', \lambda', E_B) \right). \quad (8)$$

The first sigmoid multiplies the whole expression allowing to reproduce a smooth transition from the 3D to 1D mobility of A species, which should indeed be in the leading term since they have the largest diffusion coefficient. The second sigmoid just accounts for the behavior of the B-species which are less mobile, as reflected by the weaker influence of this term.

Performing a basic fitting procedure for this function  $\delta$  leads to  $\lambda = 10$  and  $\varepsilon = 0.5$  for both sigmoid functions. This simple procedure leads to quite a reasonable fit of the simulation data as they are reproduced with about 16% discrepancy on average, with a maximum error of about a factor 2.5, while the whole set of data varies about a factor 50. Depending on the application such a precision might be sufficient or not. For example for very precise computation of dislocation loops nucleation out of irradiation, all the errors on the estimated absorption rates for monomers up to critical size clusters will cumulate and may have an impact on the overall estimated nucleation rates. On the other hand,

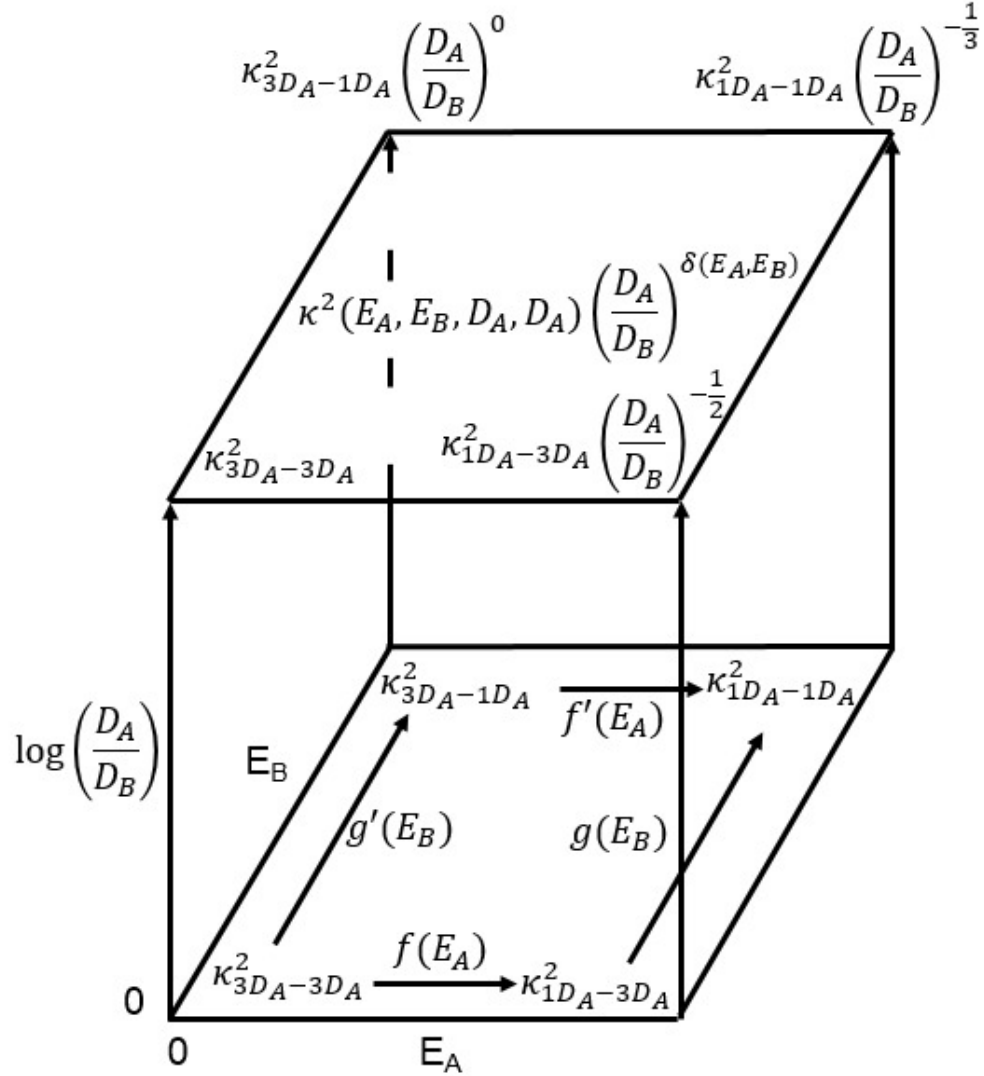


Figure 5. Schematic view of the analytical expressions for the limiting cases (corresponding the evolution of CSS along the vertical edges of the cube) for the CSS in the  $(E_A, E_B, \Delta)$  space. The functions  $f$ ,  $f'$ ,  $g$  and  $g'$  were shown to be identical by symmetry and practical arguments.

for microstructural evolution under irradiation, where the cascade cluster production may allow clusters to grow bypassing the classical nucleation path and where, due to colossal supersaturations, the expected critical radii may be extremely small, then reproducing the order of magnitude of CSS may be seen as a reasonable approximation when the purpose is to compare RECD calculation to experimental observations often having even larger intrinsic uncertainties.

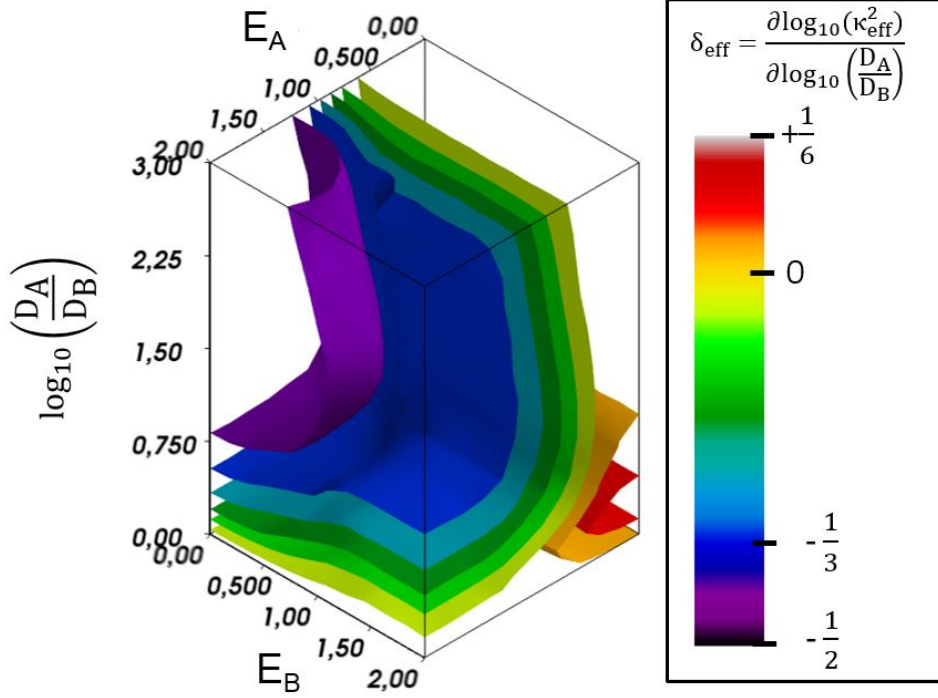


Figure 6. Effective exponents  $\delta_{\text{eff}}$  isosurfaces, allowing to identify CSS domains.

Representing the actual map of effective  $\delta$  values,

$$\delta_{\text{eff}}\left(E_A, E_B, \log_{10}\left(\frac{D_A}{D_B}\right)\right) = \frac{\partial \log_{10}(\kappa_{\text{eff}}^2)}{\partial \log_{10}\left(\frac{D_A}{D_B}\right)} \quad (9)$$

from the set of estimated CSS shows us that trying to improve the fit would require a more complex expression of the function  $\delta$  Eq. 8. This is shown on Fig. 6. The figure may also be seen as “reaction dimensionality diagram”, as it permits, basing on the values of the exponent, to identify zones in the  $(E_A, E_B, \Delta)$ -space associated with the 1D-1D type reaction (the zone delimited by the purple surface on the figure), the 1D-3D zone (the blue zone), and the rest which can be seen as a close to 3D-3D zone, apart from a small zone where  $D_A \simeq D_B$ ,  $E_A \simeq 0$ ,  $E_B \simeq 2eV$  (in red on the figure) where the exponent approaches  $1/6$ . Due to its very small extend in the  $\Delta$ -dimension this red zone wasn’t identified so far in the analysis of limiting cases, but it can be interpreted considering the analog cases highlighted in [1]

$$\frac{\partial C_A}{\partial t} = -8R\bar{D}\left(\frac{D_z}{D_\rho}\right)^{1/6} C_A C_B, \text{ for } D_z \gg D_\rho \quad (10)$$

which according to the authors of this development [17, 18] should be rightful for  $D_z \gg D_\rho$ . Using the analogy approach of the companion paper, we may take  $D_z = D_A + D_B$  and

$(C_A, C_B)$ (cm <sup>-3</sup> )	$\mathcal{C}$ Eq.11	$\varsigma$ Eq.12	$M$ Eq. 13	$Max(\kappa_{\text{eff}}^2)$ $/Min(\kappa_{\text{eff}}^2)$
$(1 \times 10^{17}, 1 \times 10^{17})$	0.98	0.087	2.37	49
$(5 \times 10^{16}, 5 \times 10^{16})$	0.97	0.080	2.38	21
$(5 \times 10^{17}, 5 \times 10^{17})$	0.98	0.078	2.36	16
$(5 \times 10^{15}, 5 \times 10^{15})$	0.97	0.095	2.37	29
$(2 \times 10^{15}, 2 \times 10^{15})$	0.97	0.105	2.37	31
$(2 \times 10^{15}, 1 \times 10^{16})$	0.97	0.097	2.39	25
$(5 \times 10^{16}, 2 \times 10^{15})$	0.98	0.091	2.35	19

Table I. Correlation coefficients  $\mathcal{C}$  for  $\log_{10}(\kappa_{\text{eff}}^2)$  versus  $\log_{10}(\kappa_{\text{fit}}^2)$  and standard deviations  $\varsigma$  of the residual of the logarithmic CSS Eq. 12. The next column is the maximum discrepancy,  $M = Max(\kappa_{\text{eff}}^2/\kappa_{\text{fit}}^2)$  over the validation data sets. For comparison the largest ratio of effective CSS  $Max(\kappa_{\text{eff}}^2)/Min(\kappa_{\text{eff}}^2)$  is given on the last column for each data set. The total radius used is always 1 nm and the box dimensions range from 300 to 4000 unit lattices depending on concentrations and  $L_{\text{min}}$ .

$D_\rho = D_B$ . Actually, the red zone is for quite small  $\Delta$  values so, if we admit that the relation also holds for moderate diffusion “anisotropy” ( $D_z \gtrsim D_\rho$ ) then, the characteristic exponent 1/6 is explained. The fact that this zone actually has a very limited range and does not extend to larger  $\Delta$  values is just due to the chosen representation: because the CSS are studied with  $(D_A + D_B)$  constant,  $D_B$  vanishes along the  $z$ -axis and the evolution is then only driven by  $E_A \simeq 0$  and its  $\delta = 0$  typical exponent.

We will now validate the semi-analytical formula outside of its fitting data set. Due to high computational cost [29] of well converged CSS for high rotation energies and low concentrations, only a limited set of concentration pairs could be used. However, we tested the formula both for equal concentrations and different ones. Results are presented on table I.

We note that the correlation coefficient for  $\log_{10}(\kappa_{\text{eff}}^2)$  versus  $\log_{10}(\kappa_{\text{fit}}^2)$

$$\mathcal{C} = Corr(\log_{10}(\kappa_{\text{eff}}^2), \log_{10}(\kappa_{\text{fit}}^2)) \quad (11)$$

are very close to one. These correlations being on decimal logarithms, it shows that, at least in terms of orders of magnitude, the formula capture almost perfectly the CSS evolution over the parameter ranges. The standard deviations on logarithms are:

$$\varsigma = \left( \frac{1}{n} \sum (\log_{10}(\kappa_{\text{fit}}^2) - \log_{10}(\kappa_{\text{eff}}^2))^2 \right)^{1/2} \quad (12)$$

and they are all of the same order (0.09) for all validation sets. This gives an estimate of the “average error” (coefficient of variation) of the semi-analytical formula: about 20%, as  $10^{0.09} \simeq 1.2$ . Globally, this is a quite good validation of the semi-analytical fit. At first sight, the quite large maximum discrepancies

$$M = \text{Max} \left( \frac{\kappa_{\text{eff}}^2}{\kappa_{\text{fit}}^2}, \frac{\kappa_{\text{fit}}^2}{\kappa_{\text{eff}}^2} \right) \quad (13)$$

displayed on table I could be considered as a source of inaccuracy. To that concern first, it should be noted that these large deviations mostly correspond to intermediate values of rotation energies, as can be seen from the isosurfaces of the residuals on Fig. 7. We can see that the residuals of logarithms

$$r = [\log_{10}(\kappa_{\text{eff}}^2) - \log_{10}(\kappa_{\text{fit}}^2)]^2 \quad (14)$$

is everywhere very close to 0 (blank zones are below 0.00746, whose square root elevated to power ten corresponds to values below the 20% average discrepancy) except when  $E_A \simeq 0.5 \text{ eV}$ ,  $E_B \simeq 0.0 \text{ eV}$  and  $\Delta \gtrsim 2$ . In that very small orange zone, it reaches 0.14 whose square root corresponds to the logarithm of the maximum discrepancy  $M$  for the first condition in table I ( $\log_{10}(2.37) \simeq \sqrt{0.14}$ ): the zones of quite high deviation from the fit are always quite small and actually correspond to transition zones.

The small extent of significant residue zones indicates that the approach consisting of entering limiting cases in the fitting formula is overall relevant and that it is mostly the choice of the transition function involving two basic logistic functions that could be improved. It appears that parity of the logistic function (it is an odd function when changing its origin to  $(\varepsilon, 1/2)$ ) does not allow to match perfectly the evolution of the effective CSS both before and after  $\varepsilon$ . This asymmetry needed to reproduce finer details of the effective CSS over the whole range may arise from the need of  $\kappa_{1DR-0}$  expressions to describe them for example near  $E_A \simeq 0.5 \text{ eV}$ ,  $E_B \simeq 0.0 \text{ eV}$  at large D-ratios. Nevertheless, to keep it as simple as possible these limiting cases were not included in the semi-analytical formula. A possibility

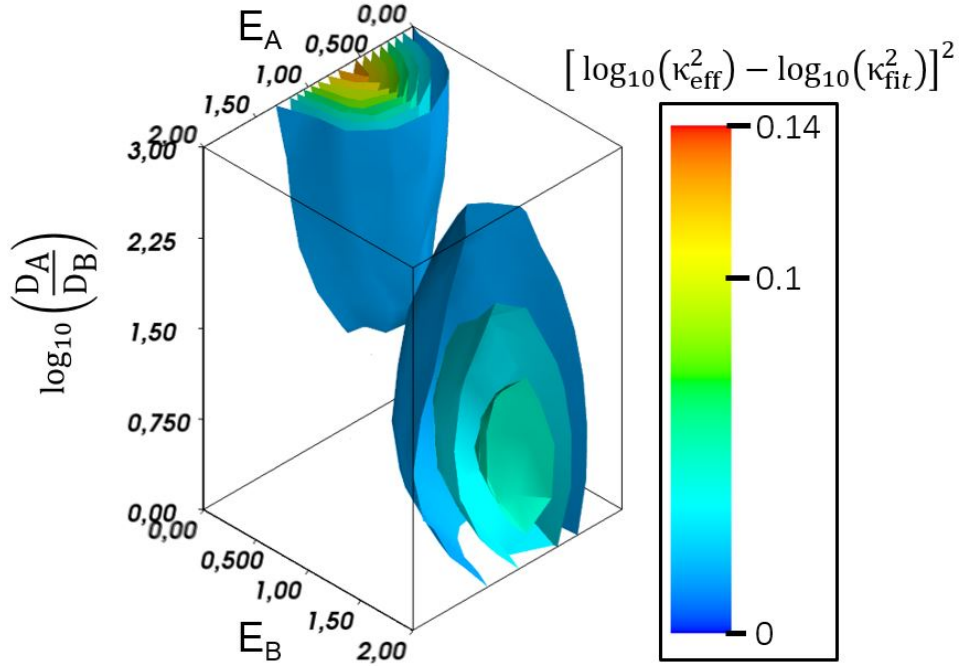


Figure 7. Isosurfaces of residuals of logarithms from Eq. 14 for the reference conditions ( $T = 573\text{ K}$ ,  $C_A = C_B = 1 \times 10^{17}\text{ cm}^{-3}$ ,  $R_A = R_B = 1\text{ nm}$ )

that does not require to include more limiting cases would be to use other functions to model the transition (asymmetric sigmoid like the generalized logistic function) which do not impose this symmetry. This was tested and achieved some partial improvement but at the cost of doubling the number of parameters. Fitting the transition zones with splines would probably be an even better option, but the number of parameters would then be as large as the product of the degree of the splines by the number of fitting point.

Notwithstanding these possible refinements of the semi-analytical fitting for transition regions, casting all possible CSS into a general formula should be seen a significant improvement of the CSS description compared to crude simplifications met in the literature consisting in approximating them with 3D CSS. Indeed we see from table I that varying rotation energies couples and diffusion ratio the CSS vary with a factor 50 as the dimensions of mobilities go from  $1D - 1D$  to  $3D - 3D$  and  $\Delta$  is below three. Thus, the approximation of treating them as purely 3D would result for the present example in overestimating also by a factor 50. This as to be compared with the 20% overall accuracy allowed by the



semi-analytical formula, that we recast here in its most explicit expansion:

$$\begin{aligned} \kappa_{\text{fit}}^2(D_A, D_B, E_A, E_B) &= \left(\frac{D_A}{D_B}\right)^{\delta(E_A, E_B)} \\ &\times \left\{ (1 - \sigma_1(E_A)) \kappa_{3D_A-3D_A}^2 + \sigma_1(E_A) \left[ (1 - \sigma_1(E_B)) \kappa_{3D_A-3D_A}^2 + \sigma_1(E_B) \kappa_{1D_A-1D_A}^2 \right] \right\} \end{aligned} \quad (15)$$

$$(16)$$

with

$$\begin{aligned} \delta(E_A, E_B) &= \sigma_2(E_A) \left( -\frac{1}{2} + \frac{1}{6} \sigma_2(E_B) \right), \\ \sigma_1(x) &= \sigma(\lambda = 8, \varepsilon = 0.2, x), \\ \sigma_2(x) &= \sigma(\lambda = 10, \varepsilon = 0.5, x), \end{aligned} \quad (17)$$

here additional simplifications have been made compared to the generic form Eq. 3:  $\kappa_{1D_A-3D_A}^2$  has been simply replaced by  $\kappa_{3D_A-3D_A}^2$ , with imperceptible loss of overall accuracy. Of course, that does not mean that these two CSS expressions have close values in general (it is clearly wrong for small  $\Delta$ ), but rather that most of their relative evolution for increasing  $\Delta$  can be cast into a leading term, the D-ratio power delta term (or scaling term). It is also interesting to note that quite counter-intuitively, simple reductions of the dimensionality of the mobilities are often misleading whereas dimensionality equivalences are relevant: having both species 1D-migrating and  $D_B$  as small as  $D_B/D_A = 10^{-3}$  does not allow to treat  $B$  as immobile, as the effective CSS is far from the analytical  $1D - 0$  CSS, whereas it matches well the  $2D - 0$  CSS with proper accounting of scaling term. This important point will be further investigated in the next section.

Finally, note that this semi-analytical formula is directly valid only at  $T_0 = 573K$ . As such, it is also bound to the first nearest neighbor jump distance used in the OKMC simulations for the fitting set. To extend it to other temperatures and other lattices than BCC, a simple modification is proposed in the Annex C.

## B. Closure of the CSS domains

In the previous section, we noted that even for diffusion coefficients ratios as low as  $\mathcal{D} = 10^{-3}$ , the least mobile specie may not be treated as immobile, as the most relevant

analytical CSS is the properly corrected  $1D - 1D$  expression. It is important for modeling concerns to investigate to which extends this holds, and what is the typical diffusion ratio where the  $1D - 0$  CSS starts to be more relevant. The semi-analytical formula that we have established allows for reasonably accurate estimation of CSS depending on  $(E_A, E_B, \Delta)$ , but due to its numerical cost, the fitting set was limited to  $0 \leq \Delta \leq 3$ . On that part of the  $(E_A, E_B, \Delta)$ -space, the two main absorption-rate domains are clearly visible ( $3D - 1D$  and  $1D - 1D$ ) but none of them are closed at  $\Delta = 3$ . As a consequence the validity of the formula as such is restricted to that range, because there must be some D-ratio above which  $B$  should be considered as immobile and the CSS tend to  $3D - 0$  and  $1D - 0$  expressions respectively. For the former, the transition does not need to be explicitly accounted as  $3D - 3D$  CSS expressions encompasses the case  $D_B = 0$ , whereas for the  $1D - 1D$  to  $1D - 0$  transition the reaction rates do not even have the same reaction order. Thus the range of  $\Delta$  was extended to  $\Delta = 6$  in a new calculation set where the sampling criteria were slightly relaxed. As displayed on Fig. 8 the domain for  $1D - 3D$  CSS now closes by  $\Delta = 4.5$  and that of  $1D - 1D$  CSS closes about 5. From  $\log_{10}(D_A/D_B) = 3.75$  to 7.5 some isosurfaces are wavy because the sampling set is smaller than for the former conditions. This could not be easily improved as the present result already required about 2.2 million CPU hours on Xeon Sandy Bridge 2.6 GHz cores. Being more precise on the closures in the  $(E_A, E_B, \Delta)$ -space would require quite a lot more computational resources, so we should rather focus on more restricted case, the  $(E_A = 2 \text{ eV}, E_B = 2 \text{ eV})$  case.

To that end, a few sets of simulations (for a few  $(C, R)$  couples,  $C = C_A = C_B$ ) for  $\Delta$  ranging from 0 to 9 was ran. The results are shown on Fig. 9 which represents the normalized quantity:

$$Y(\Delta) = \frac{\kappa_{\text{eff}}^2 - \kappa_{1D-0}^2}{\kappa_{2D-0}^2 - \kappa_{1D-0}^2}. \quad (18)$$

This quantity is equal to one when  $\kappa_{\text{eff}}^2 = \kappa_{2D-0}^2$  and when it tends to zero then  $\kappa_{\text{eff}}^2$  tends to  $\kappa_{1D-0}^2$ . When varying concentrations and radii, it helps to check if a common trend for the transition towards  $1D - 0$  stands out, when concentration couples vary. We see that it is indeed the case for the typical volume fraction conditions investigated. The question whether this simple behavior extends to a much wider range of  $(C_A, C_B, R)$  conditions could be delicate and is not addressed here. We rather focus on proposing a practical correction for the vanishing scaling factor  $(\mathcal{D})^{-1/3}$  that would clearly lead to an underestimation of

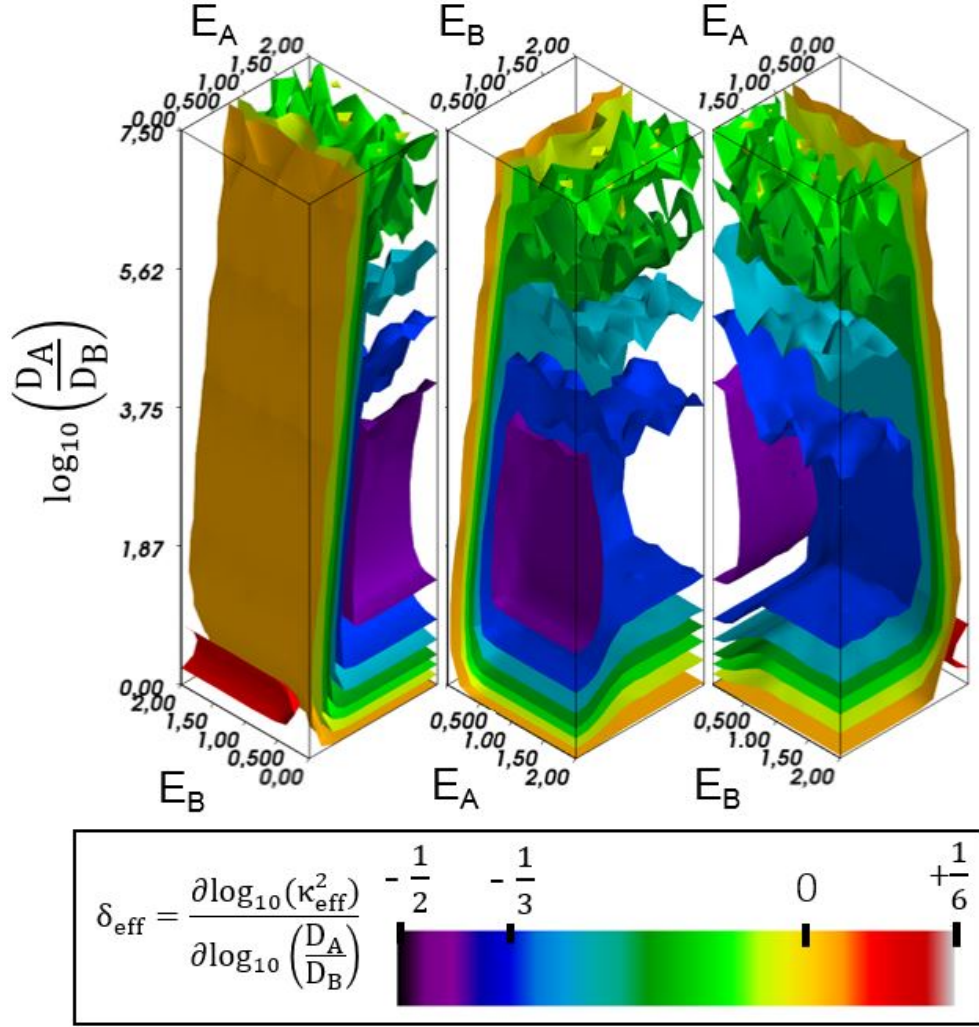


Figure 8. Three views of the effective exponents  $\delta_{\text{eff}}$  isosurfaces.

CSS from some point when  $\Delta$  is small. For the investigated conditions, the  $1D - 1D$  to  $1D - 0$  transition happens to follow a common trend that is well fitted by the generalized sigmoid,

$$Y_{\text{fit}}(\Delta) = a - \frac{b}{(c + d \exp(e\Delta - f))^g} \quad (19)$$

with  $a = 0.0071, b = -1.26, c = 2.23, d = 0.932, e = 3.81, f = 0.98, g = 0.26$  as shown on Fig. 9.

From the representation of  $\kappa_{\text{eff}}^2/\kappa_{1D-0}^2$  at Fig. 10, we can conclude that, depending on the  $C$  and  $R$  the effective CSS reaches the analytical  $\kappa_{1D-0}^2$  within a typical 5-10 % uncertainty of estimates by  $5 < \Delta < 6$ , except for the blue curve whose atypical behavior is explained

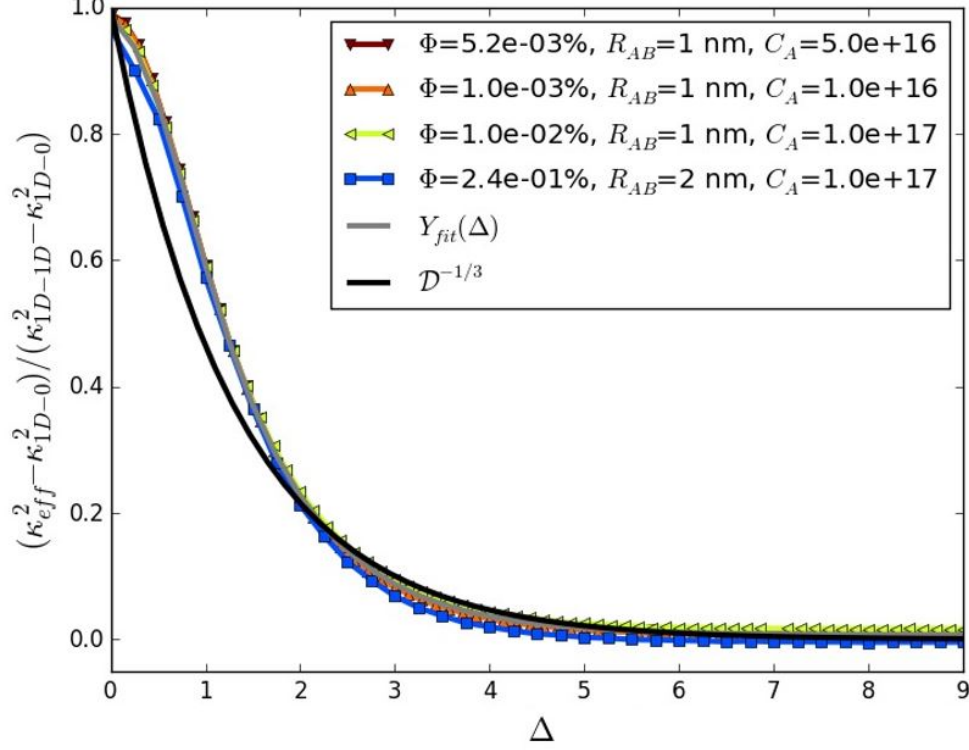


Figure 9. Transition of the normalized CSS from  $1D - 1D$  to  $1D - 0$  for four different conditions. The generalized sigmoid fit follows Eq. 19. In the caption,  $\Phi$  represents the defects volume fractions and the concentrations  $C_A = C_B$  are given in  $\text{cm}^{-3}$ .

by a very large volume fraction. Formally, we can identify a critical  $\Delta$  value by equating the  $1D-0$  and  $1D-1D$  CSS which leads to

$$\Delta^* = -3 \log_{10} \left( \frac{3}{\bar{\alpha}} R^3 C \right), \quad (20)$$

where  $\bar{\alpha} \simeq \frac{4}{\ln(\pi^2 C R^3 / 2)}$  is the usual parameter entering in the  $1D - 1D$  CSS expression [1]. The evaluation of  $\Delta^*$  for the conditions of Fig. 10 leads to values mostly between 6 and 8, which corresponds reasonably well to the critical values from the figure. Nevertheless the approach from the Eq.20 and the actual evolution towards the critical values do not compare further: it is clear that the transition is very gradual and that both  $1D - 1D$  and  $1D - 0$  mechanisms operate simultaneously even above the critical value. To the simplest way, the cross-over between mobile and fixed sinks related CSS may be cast with semi-analytical

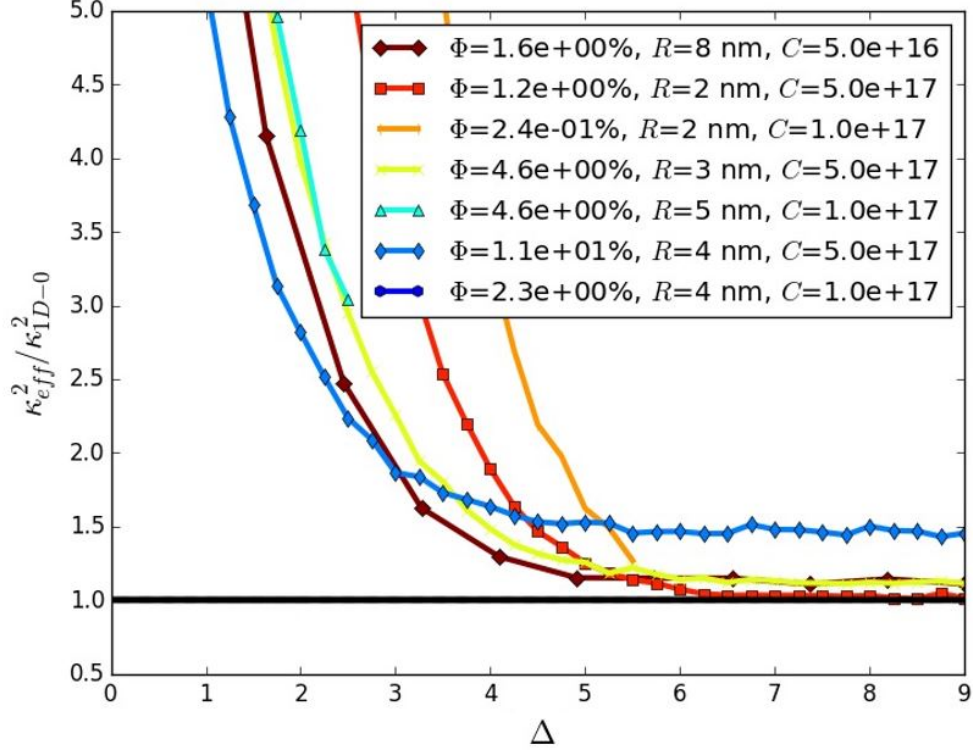


Figure 10. Convergence of the ratio of the effective CSS over the analytical  $1D-0$  CSS for different conditions. In the legend,  $\Phi$  represents the volume fractions and the concentrations are given in  $\text{cm}^{-3}$ .

formula as:

$$\text{Max} \left( \kappa_{\text{fit}}^2(C_A, C_B, R, E_A, E_B, D_A, D_B), \right. \quad (21)$$

$$\left. \kappa_{1DR-0}^2(C_A, C_B, R, E_A, D_A) \right). \quad (22)$$

A more elaborated way of reproducing the transition would be to use the fit Eq. 19 and replace it back in Eq. 18:

$$\kappa_{\text{fit}}^2 = Y_{\text{fit}}(\Delta)(\kappa_{2D-0}^2 - \kappa_{1D-0}^2) + \kappa_{1D-0}^2, \quad (23)$$

but this should be valid only for pure  $1D-1D$  and establishing a  $Y_{\text{fit}}$  function valid for any rotation energy couple would require a more complex function with much more parameters.

### III. APPLICATION TO CLUSTER DYNAMICS

We now briefly expose the results of the application of the semi-analytical CSS on cluster dynamics simulations. This development allows to properly account for the agglomeration of defect clusters with mixed 1D/3D mobility i.e. any couple of rotation energies. Some additional technical details on the implementation in the code CRESCENDO [13] can be found in the corresponding section of paper I. Here we focus on the ability of the present extension to reproduce an OKMC microstructure simulation close to the state-of-art in terms of complexity of random-walks. A concentration of  $2 \times 10^{16} \text{ cm}^{-3}$  interstitial monomers is initially placed in a quasi-cubic box of about 2000 lattice constants length. The parameterization will allow the formed clusters to be mobile up to the size 60. Increasing cluster content from 1 to 60 monomers, the diffusion coefficients are decreasing according to the power law  $n^{2/3}$  from  $1.8 \times 10^{-5}$  to  $1.16 \times 10^{-6}$  and their rotation energies increase from 0 to 2 eV (linearly up to size 12 and then the energy reaches a plateau value of constant value of 2 eV). Regarding rotation energies, these parameters are intended to sketch some state-of-the-art OKMC parameterizations found in the literature [24]. To be comparable with RECD, OKMC simulation must consist of hundreds to thousands of runs with different random seeds: a given OKMC run generally ends up with a few clusters resulting in a sparse distribution, while in RECD significant concentrations of defects are often found in quite smeared and continuous distributions. Figure 11 shows the comparison between the two simulation methods. It is worth mentioned that, although the set of one thousand lengthy OKMC runs represent a considerable amount of computer resources compared to the RECD simulation (OKMC requires here several millions times more individual CPU time than RECD), it is still not enough to fully characterize the distribution as it appears discontinuous due to the lack of sampling at the greatest sizes. Nevertheless, on the existing OKMC points the agreement with RECD is completely satisfactory, apart from the fact that at the intermediate simulation times the OKMC distribution is rougher and matches RECD distribution with some delay. Aside mentioned sampling limitations, this discrepancy is also quite likely to be a small box size effect: at intermediate evolution times, the peak of the cluster distribution is quite spread and it is barely above the minimum OKMC concentration for a single run ( $C_{min} = 1/V_{box}$ , the dashed line of Fig. 11). This clearly generates box size effects that are quite challenging to overcome with reasonable computational resources.

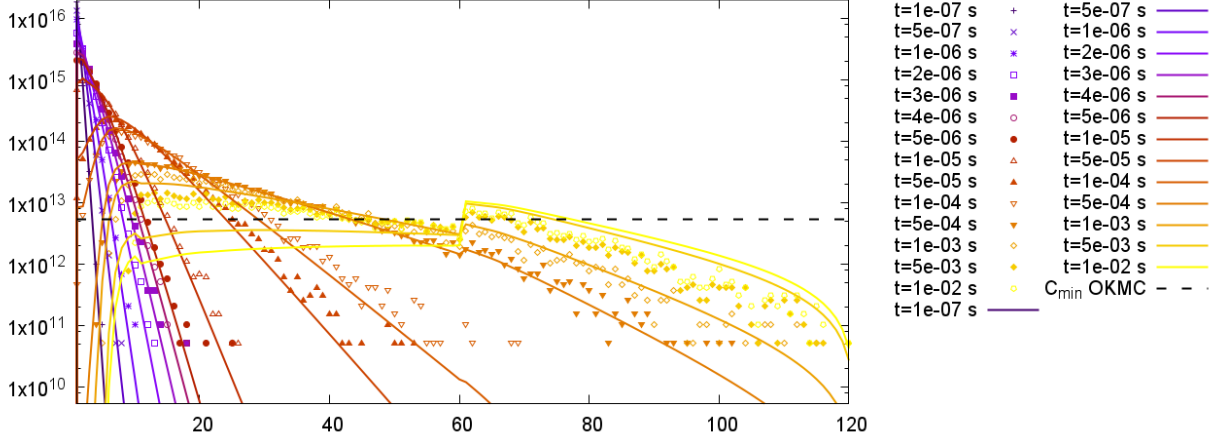


Figure 11. Defect clusters distribution (x-axis is the cluster size in number of monomers, and the y-axis in the cluster concentration in  $\text{cm}^3$ ). Starting from a population of  $2 \times 10^{16} \text{ cm}^{-3}$  SIA, the time evolution of the defect clusters population with mixed mobility was obtained by averaging one thousand OKMC runs (points). The comparison with RECD calculation is given by the continuous lines. The dashed line represents the minimum concentration (the inverse of the box volume) accountable in OKMC simulations.

#### IV. DISCUSSION: THE RELEVANCE OF MIXED MOBILITY SINKS STRENGTH TO DISLOCATION LOOP EVOLUTION MODELING

Dislocation loops are complex objects whose mobilities are driven by the singular character of the stress field they wear. This is also the physical origin of the rotation energies [19] (that we have taken here as black box parameter) as the rotation phenomenon shares some similarities with cross-slip, but with specific attempt frequencies and activation energies due to the closed chain nature of loops [20]. A consequence of this is that the rotation probability of a loop may not always bear a simple parameterization with a fixed rotation energy that only depends on its size: it may also depend on the elastic fields that surrounds it. By construction, in cluster dynamics we can only hope to treat these types of spatial effects in a very indirect way and this would be at the cost of quite heavy modifications of the original formalism.

Another important phenomenon is the trapping of loop by chemical heterogeneities. Carbon and nitrogen, even at a few tens of ppm concentrations can have a huge impact on mobility of loops in ferritic materials at moderate temperature. Cottrell atmospheres of

carbon atoms may form in the tensile zone of dislocation loops thus lowering the effective mobility of loops, and in the presence of vacancies, vacancy-carbon complexes may form [21] and trap dislocation loops for long times. The effective migration energies of loops are thus significantly increased by a function of the trap-loop binding energy. In other words, untrapped species are expected to be in lower number densities than trapped ones in many conditions, so, at first sight, one may believe that  $1DR - 1DR$  CSS may play a secondary role in the microstructure kinetics compared to  $1DR - 0$  ones. But we shall keep in mind that:

- At high temperature, the trapping is less effective. There could even exist a cross-over between trapping and its opposite effect, the elastic confinement of loops by over-sized solute atoms [22].
- The vicinity of fixed sinks (dislocation network and grain boundaries) are often depleted of traps. It is indeed in these regions that greater populations of small dislocation loops (in the form of TEM “black dots”) can be seen in complex alloys with many solutes and impurities such as industrial RPV steels at moderate doses. This is a local effect but nevertheless crucial as it conditions the local mobility of dislocation which is a key point for mechanical properties evolution under irradiation.
- Even if loops spend most of the time trapped, clusters from the resulting smaller population of untrapped loops may react quite intensively and depending on the detailed conditions create a specific population.
- At least from some point, the traps should be saturated and the new free defect clusters produced in cascades should be more likely to interact with other mobile clusters, than to be trapped. In the parameters set taken as an example in this study (see table II) the single interstitials are considered as 3D-mobile and from size 3 they start having a mixed mobility. Note also, that in other systems, the mono-interstitials may be crowdions and exhibit pure 1D-motion [23]. In all these cases the  $1DR - 1DR$  CSS must be taken into account.
- As we have seen in section II B, even with six orders of magnitude difference for the diffusion coefficients of two interacting 1D-mobile species, the  $1DR - 0$  CSS approximation is a serious underestimation of the effective CSS, contrary to the adapted  $1D - 1D$



expression. We can be more quantitative for this last but not least point: a popular way of accounting for trapping, inspired by the developments of Krishan [15] and others, is to simply lower the effective diffusion coefficient by a factor  $\exp(-E_{\text{trap}}/k_B T)$ , where  $E_{\text{trap}}$  is the binding energy between the cluster and the trap. Actually, this corresponds to a lower bound for the effective diffusion coefficient as the trapping efficiency is assumed to be ideal. At 573 K, a trapping energy around 0.68 eV corresponds to the factor  $10^{-6}$  reduction of effective mobility. So, below this threshold trapping energy, a weakly trapped cluster should definitely be considered as mobile with respect a free clusters of the same size, as the CSS error resulting from treating the interaction as  $1D - 0$  would be large according to figure 10. There are several defect sizes complying with this condition in the parameterization exemplified in the appendix's table II: these are the smallest clusters but also, the most mobile and thus the most influential on the kinetics.

With these considerations in mind, mobile clusters aggregation (by diffusion of both reaction partners) should, at least be considered as a channel for loop growth competing with Ostwald ripening, and could even overtake it in specific conditions. In a nutshell, for a population of trapped clusters, Ostwald ripening will dominate only if the cluster dissolution rate is higher than the de-trapping rate. For the parameterization exemplified in the annex, trapping energies of loops range from 0.17 to 0.6 eV below a cluster size threshold value [30] and then 1.1 eV above the threshold. The corresponding binding energies values are always much higher than trapping energies at each cluster size (binding energies typically range 0.87 eV up to the formation energy of interstitial which is extremely high). So if the raw diffusion coefficients of interstitial clusters are comparable in terms of orders of magnitude to that of the monomer, then the loops will be more likely to untrap rather than dissolve and feed the Ostwald ripening process. Of course we may not prematurely conclude that aggregation always prevails, because high diffusion also promotes higher effective rates of emission (absorption rates appear in emission rates), but we stress out that the competition between the two processes must be considered. This shed new light on the range of validity of some of the major nucleation theories: in the LSW formalism, both reaction channels are indeed considered but the formulation of agglomeration rates restricts its application to 3D mobilities. Since no expression for absorption rates involving two  $1DR$  species with arbitrary diffusion coefficients was available, the applicability of general results on growth asymptotics

to these cases was unclear. Now we see that, once proper corrections are applied, absorption rates between such species lead to second order kinetics rates just as 3D ones, and classical results may be qualitatively valid.

## V. SUMMARY AND CONCLUSIONS

Because the CSS dependence on concentrations, radii, diffusion coefficient and rotation energies is unknown and non-linear, complete fitting of CSS on all of its variables may represent quite a formidable task: any decent gridding would probably require millions of conditions, all of which having quite different convergence behavior as the estimated CSS will span over several orders of magnitude. To tackle this problem of the large set of conditions, the proposed approach is the following: fixing the defect concentrations and the radii, we generated a first data set gridding on the diffusion coefficient ratio and on the rotation energies. Then, we combined the analytical expressions developed in paper I [1] as limiting cases, thus allowing us to extend the expressions to arbitrary concentrations and radii, as was further check by analysis of the residuals. The transition between the limiting cases can be modeled by two combinations of sigmoids: a first combination of sigmoids is used to describe the transition between the CSS when  $D_A = D_B$ , and the second couple of sigmoids is intended to reproduce the presence of the quite distinct mobility domains (consistently with the limiting cases) which appear clearly when mapping the effective exponents of the diffusion ratio correcting factor. This term appears to be most crucial to capture the many order of magnitudes over which the CSS vary when the diffusion coefficient ratio goes from one to small values ( $\Delta$  going from 0 to large values). We also looked for the point from which the slowest specie should actually be considered as immobile in the reaction. The CSS with respect to a fixed sink would then become more relevant. This limit happens to be surprisingly low, which stresses out the necessity to use the  $1DR - 1DR$  CSS fit up to very small diffusion ratios. This should also be the case for the most important defect cluster couples (those mostly produced by cascades and that actually lead the dynamics) in the most typical irradiation situation discussed and would still hold when effective diffusion coefficients are be considerably lowered by trapping. The relevance of  $1DR - 1DR$  reactions is thought to be quite general: depending on detailed conditions and especially on temperature, aggregation of mobile clusters may compete with Ostwald ripening. Finally,

in the application of the RECD implementation, an in-depth validation of the formula was allowed thanks to a massive set of OKMC simulations with large box sizes requiring at least millions times more CPU time than RECD. As in moderate stiffness cases, RECD numerical schemes allow for very large time steps, this opens the way to very long-term (decades of physical time) simulations of the microstructure evolution fully accounting for the mixed mobility defect clusters which is intrinsically out of reach of any event-based method such as KMC.

## VI. ACKNOWLEDGEMENTS

Lorenzo Malerba is warmly acknowledged for initially pointing out the necessity of considering the mixed mobilities in KMC simulations, which initiated this work on their RECD counterpart, as well as Christophe Domain who additionally performed a benchmarking with its own implementation of effective CSS calculation within LAKIMOCA. Jean-Paul Crocombette is thanked for his suggestion to think about a “phase-diagram”-like representation of the CSS evolution with the mobility parameter. Thomas Jourdan is also acknowledged for collaboration on the implementation into the code CRESCENDO.

## VII. FUNDING

This project has received funding from the Euratom research and training program 2014-2018 under grant agreement No 661913 (SOTERIA).

- 
- [1] G. Adjanor Complete characterization of sink-strengths for 1D to 3D mobilities of defect clusters. I. Extension to diffusion anisotropy analog cases. *ArXiv e-print* 1808.10362, cond-mat.mtrl-sci, August 2018, <https://arxiv.org/abs/1808.10362>
  - [2] L. Malerba, C.S. Becquart, and C. Domain. Object kinetic Monte Carlo study of sink strengths. *Journal of Nuclear Materials*, 360(2):159–169, 2007.
  - [3] C. Domain, C. S. Becquart, and L. Malerba. Simulation of radiation damage in Fe alloys: An object kinetic Monte Carlo approach. *Journal of Nuclear Materials*, 335(1):121–145, 2004.

- [4] A.V. Barashev, S.I. Golubov, and H. Trinkaus. Reaction kinetics of glissile interstitial clusters in a crystal containing voids and dislocations. *Philosophical Magazine A*, 81(10):2515–2532, 2001.
- [5] H. Trinkaus, H.L. Heinisch, A.V. Barashev, S.I. Golubov, and B. Singh. 1D to 3D diffusion-reaction kinetics of defects in crystals. *Physical Review B*, 66(6):060105, 2002.
- [6] H.L. Heinisch, B.N. Singh, and S.I. Golubov. Kinetic Monte Carlo studies of the effects of Burgers vector changes on the reaction kinetics of one-dimensionally gliding interstitial clusters. *Journal of Nuclear Materials*, 276(13):59 – 64, 2000.
- [7] S. Redner. *A Guide to First-Passage Processes*. Cambridge, 2002.
- [8] P.L. Krapivsky, S. Redner, and E. Ben-Naim. *A kinetic view of statistical physics*. Cambridge University Press, 2010.
- [9] T. Amino, K. Arakawa, and H. Mori. Reaction rate between 1D migrating self-interstitial atoms: an examination by kinetic Monte Carlo simulation. *Philosophical Magazine*, 91(24):3276–3289, 2011.
- [10] K. Arakawa, K. Ono, M. Isshiki, K. Mimura, M. Uchikoshi, and H. Mori. Observation of the one-dimensional diffusion of nanometer-sized dislocation loops. *Science (New York, N.Y.)*, 318(5852):956–959, 2007.
- [11] T. Hamaoka, Y. Satoh, and H. Matsui. One-dimensional motion of self-interstitial atom clusters in A533B steel observed using a high-voltage electron microscope. *Journal of Nuclear Materials*, 399(1):26–31, 2010.
- [12] T. Hamaoka, Y. Satoh, and H. Matsui. One-dimensional motion of interstitial clusters in iron-based binary alloys observed using a high-voltage electron microscope. *Journal of Nuclear Materials*, 433(1-3):180–187, 2013.
- [13] T. Jourdan, G. Bencteux, and G. Adjanor. Efficient simulation of kinetics of radiation induced defects: A cluster dynamics approach. *Journal of Nuclear Materials*, 444(1-3):298–313, 2014.
- [14] L. Ratke. Simultaneous coarsening of dispersions by growth and coagulation. *Journal of Colloid and Interface Science*, 119, 1987.
- [15] K. Krishan and N.N. Thieu. Effect of Ti addition on swelling in 316 stainless steel under HVEM conditions. *Radiation Effects*, 100(3-4):249–261, 1987.
- [16] P. Ramachandran and G. Varoquaux. Mayavi: 3D visualization of scientific data. *Computing in Science & Engineering*, 13(2):40–51, 2011.

- [17] U. Gösele and A. Seeger. Theory of bimolecular reaction rates limited by anisotropic diffusion. *Philosophical Magazine*, 34(2):177–193, 1976.
- [18] C.H. Woo. Effects of Anisotropic Diffusion on Irradiation Deformation. *Radiation-Induced Changes in Microstructure: 13th International Symposium (PART I), ASTM STP 955*, pages 70–89, 1987.
- [19] T. Okita, S. Fujita, Y. Yang, and N. Sekimura. Interaction mechanisms of glissile loops in FCC systems by the elastic theory. *Journal of Nuclear Materials*, 386:188–190, 2009.
- [20] S. L. Dudarev, M. R. Gilbert, K. Arakawa, H. Mori, Z. Yao, M. L. Jenkins, and P. M. Derlet. Langevin model for real-time Brownian dynamics of interacting nanodefects in irradiated metals. *Physical Review B - Condensed Matter and Materials Physics*, 81(22):224107, 2010.
- [21] N. Anento and A. Serra. Carbon-vacancy complexes as traps for self-interstitial clusters in Fe-C alloys. *Journal of Nuclear Materials*, 440(1):236–242, 2013.
- [22] T.S. Hudson, S.L. Dudarev, M.-J. Caturla, and A.P. Sutton. Effects of elastic interactions on post-cascade radiation damage evolution in kinetic Monte Carlo simulations. *Philosophical Magazine*, 85(4-7):661–675, 2005.
- [23] T. Amino, K. Arakawa, and H. Mori. Detection of one-dimensional migration of single self-interstitial atoms in tungsten using high-voltage electron microscopy. *Scientific reports*, 6:26099, 2016.
- [24] M. Chiapetto, L. Malerba, and C. S. Becquart. Nanostructure evolution under irradiation in FeMnNi alloys: A grey alloy object kinetic Monte Carlo model. *Journal of Nuclear Materials*, 462:91–99, 2015.
- [25] L. Malerba, private communication
- [26] The most simple lattice model that we can choose is simple cubic so the number of atomic sites per unit cell (equal to one in this case) does not appear.
- [27] With this same approximation, Eq. B2 is identically obtained assuming a Poisson distribution rather than binomial one.
- [28] Here, by naive parallelization is meant averaging over many different too short stochastic runs with different initial defect positions in an attempt to circumvent a too long CPU time for a single run.
- [29] Note that although the computing strategies adopted here allowed to reduce by orders of magnitudes the required computational effort, the total amount of CPU time for the production

of the fitting and validation data sets represents more than 14 millions of CPU hours on Xeon Sandy Bridge 2.6 GHz cores.

[30] Interestingly, the study of Chiapetto *et al.* [24] shows that the threshold size for trapping energies to exceed 0.6 eV is a key parameter to accurately reproduce experimental sizes and number densities of loops. The comparison with the 0.68 eV trapping energy for the transition from  $1D - 1D$  to  $1D - 0$  is quite appealing.

## Appendix A: General scheme for effective sink-strengths computations

In the case general case where both reaction partners  $A$  and  $B$  can be mobile, we expect non-trivial dependencies of absorption rates on the couple of concentrations ( $C_A$ ,  $C_B$ ) and substantial dependence on the diffusion coefficient ratio  $\mathcal{D} = D_B/D_A$ . The effective CSS calculation should then be done with large numbers of clusters in the simulation box to allow for more flexibility in the choice of concentrations and better physical accuracy of estimates.

Malerba *et al.* [2] used the OKMC code LAKIMOCA [3] to compare effective to the  $1DR - 0$  CSS analytical formula [4–6]. In that study, effective  $1DR - 0$  sink-strengths were estimated using a parameterization for interstitial type objects performing 1D-jumps along one over the four variants of the glide directions of the  $1/2\langle 111 \rangle$  family. Changes of the glide direction (rotations) were chosen among all other possible stochastic events proportionally to their respective frequencies, and so that the average distance covered between two rotations is  $\ell_{ch} = d_j \sqrt{\exp(E/k_B T)}$  on average (where  $d_j$  is the jump distance,  $E$  is defined as the rotation energy,  $k_B$  is Boltzmann’s constant and  $T$  the temperature). The effective CSS calculation then consists in placing one sink, then operating many OKMC jump events for mobile clusters and gathering very large statistics to estimate the average number of jumps before a contact between an  $A$ -particle and a  $B$  type one. Yet, for more general CSS estimations, such a procedure has some limitations: the concentration of both species are equal so exclusion volume effects (see for instance Redner *et al.* [7, 8]) between same type particles cannot be accounted for. On top of that, having a single sink in periodic box, the resulting CSS corresponds to the case of a cubic mesh of sinks instead of a random distribution of them. Nevertheless, at least the first limitation is not critical for the authors’ purpose since there is no need to vary both concentrations when one of the reaction partners is immobile and the analytical form of CSS to validate is known *a priori*. Conversely, for

the more general framework of our study without *a priori* knowledge of the general CSS expressions, a new procedure for estimating effective CSS has to be established.

The general scheme can be described as follows:

1. One places  $N_A = C_A V$  and  $N_B = C_B V$  A and B species at random positions in the box of volume  $V$ , but away from reaction distances ( $R = R_A + R_B$ ,  $R_{AA} = 2R_A$ ,  $R_{BB} = 2R_B$ ) of all other objects.
2. All defects may jump sequentially according to the OKMC algorithm and to their mobility characteristics ( $D_A$ ,  $D_B$ ,  $E_A$ ,  $E_B$ ), until one object enters a reaction volume.
3. Once an heterotypic reaction (i.e. an  $A - B$  reaction) occurs, the time span from the previous reaction of this type is recorded. Then, one of the two species is moved to a random place of the box, away from all possible reactions' distances. This is necessary to keep the concentration of species constant, while preventing from overestimating absorption rates if the reacting defect pair would not be separated after the reaction time is recorded.
4. Once an homotypic reaction ( $A - A$  or  $B - B$  reactions) should occur, the associated time span is not recorded, and the reactions partners are randomly replaced away from any capture distance, as in the previous case. Without this precaution, the defects capture volumes would overlap and the sink strength would be underestimated.
5. Periodically when, on average, each defect should have reacted a few times, all the defects are randomly placed in the box again, thus allowing sampling of initial distributions of defects whose effects can be especially important at low volume fractions of 1D-mobile species [7].

This procedure shares some common points with that of Amino *et al.* [9] but, together with convergence criteria that will follow, it is meant to be more robust for the wide range of mobility parameters  $S = (C_A, R_A, D_A, E_A, C_B, R_B, D_B, E_B)$  that we wish to explore in this paper.

## Appendix B: Search for general simulation setup and convergence criteria

According to transmission electron microscopy (TEM) observations [10–12], once they are untrapped, even large (here we mean visible in conventional TEM) dislocation loops can have a large mobility. Some state-of-the-art OKMC parameterizations like that of Malerba *et al.* [25] were aimed at reproducing these experimental observations: the jump frequency of loop object is essentially a decreasing function of the loop size and is given by the product of the exponential of a migration energy (which is comparable to the Peierls barrier as mobility of large loops is can be seen as glide of a circular dislocation) and an attempt frequency. Given this jump model, the evolution of SIA clusters’ diffusion coefficients from monomers to nanometric loops will span over several orders of magnitude. Even if small, mobilities of large loops can be crucial to reproduce loop coarsening kinetics which can be driven either by Ostwald type ripening ([13]) or by aggregation of mutually mobile species ([14], also term as “collision” in the literature). In order to account for these phenomena with RECD, the basic ingredients are the absorption rates of all combinations of reacting species whose D-ratios span of over a large range. Values of attempt frequencies  $\nu$ , migration energies  $E^m$ , rotation energies  $E$  for different interstitial cluster sizes (number of SIA,  $n$ ) from one typical parameterization of Malerba *et al.*’s are given in table II. This gives us a hit of the typical orders of magnitudes and variations amplitudes of these physical parameters for BCC iron.

It should be stressed out that to have a physically relevant parameterization of loops’ mobility, it would be very important to model at the same time the trapping centers that significantly reduces the loop’s effective diffusion coefficients, otherwise all loops would probably annihilate at the surfaces and none would be visible. Typical traps are impurities, or carbon-vacancy complexes in the referred parameterization. Nevertheless, this feature of the original model is not accounted for in the present study as it focuses on cluster-cluster interactions and not traps although they wouldn’t be a major difficulty to include them in the final RECD parameterization as far as their CSS formulation is concerned.

In this study, we vary the D-ratios from  $10^{-3}$  to 1. Rotation energies values span from 0 for an interstitial monomer which is here considered as fully 3D-mobile, to 2 eV which, for moderate defect volume fractions and temperatures, can be considered as sufficient to ensure a completely one dimensional trajectory before absorption. We see that if we cannot make any *a priori* assumptions on the dependence of CSS on defect parameters



$n$	$\nu$ ( $s^{-1}$ )	$E^m$ ( $eV$ )	$D$ ( $cm^2s^{-1}$ )	$E$ ( $eV$ )
1	$8.07 \times 10^{13}$	0.31	$8.31 \times 10^{-3}$	0
2	$3.41 \times 10^{14}$	0.42	$3.51 \times 10^{-2}$	0
3	$1.17 \times 10^{13}$	0.42	$1.21 \times 10^{-3}$	0.2
4	$1.19 \times 10^{13}$	0.80	$1.23 \times 10^{-3}$	0.4
5	$1.56 \times 10^{12}$	0.1	$1.60 \times 10^{-4}$	0.6
6	$1.71 \times 10^{12}$	0.2	$1.76 \times 10^{-4}$	0.8
7	$1.71 \times 10^{12}$	0.2	$1.76 \times 10^{-4}$	1.0
8	$1.53 \times 10^{12}$	0.2	$1.58 \times 10^{-4}$	1.2
9	$1.39 \times 10^{12}$	0.2	$1.43 \times 10^{-4}$	1.4
10	$1.28 \times 10^{12}$	0.2	$1.32 \times 10^{-4}$	1.6
11	$1.19 \times 10^{12}$	0.2	$1.22 \times 10^{-4}$	1.8
12	$1.11 \times 10^{12}$	0.2	$1.14 \times 10^{-4}$	2.0
$\vdots$	$\vdots$	0.2	$\vdots$	2.0
60	$2.45 \times 10^{11}$	0.2	$3.15 \times 10^{-5}$	2.0

Table II. Mobility parameters for interstitial clusters in one typical parameterization proposed by Malerba et al.

for an arbitrary couple of values  $(E_A, E_B)$ , the required number of calculations can be quite large. Indeed, if we would grid on only six values for each of the eight parameters  $(C_A, R_A, D_A, E_A), (C_B, R_B, D_B, E_B)$ , there would be millions of parameter combinations to consider. On top of that, for each of it, the CPU time required for convergence is very variable and its spans from minutes to weeks. Thus, our first task should be to take simplifying assumptions to limit the number of conditions and our second task to study the conditions for convergence of mixed mobility CSS.

### 1. Simplifying assumption on the capture distance

The first important assumption is that the radius dependencies can be cast into the single parameter  $R = R_A + R_B$ , as it appears in the previously established analytical expression

CSS from the companion paper. This approximation should be well verified when  $R_A \simeq R_B$ . If  $R_A \ll R_B$  it can be questioned because, if homotypic reactions are prevented, then there will be a coexistence of zones with high concentrations of A-species with depleted ones while B-species will tend to be evenly-spaced. As the simplifying assumption on the capture distances happens to be numerically well validated for  $3D-3D$ ,  $1D-3D$  and  $1D-1D$  CSS (figures not shown for brevity) we may not question it much further in the general case. For 1D mobiles, summing the radii should be *a priori* more questionable as they are even more prone to establish depleted zones, but it also happened to be very well validated.

## 2. Technicalities of the simulation box size setup

Because 1D-mobility may be far less efficient than the 3D one to sample the space (as reflected considering roughly  $\kappa_{1D-0}^2 \propto \kappa_{3D-0}^2 \Phi$  [1],  $\Phi$  being a volume fraction) very large simulation boxes may be required. As Malerba and co-workers pointed out [2], taking three different prime numbers for box dimensions is sufficient to prevent a mobile with  $\langle 111 \rangle$  glide direction to stay confined in the diagonal or any periodic path as it happens when having periodic boundary conditions in a box whose dimensions have common divisors. Nevertheless, at variance with the authors' case where only sink concentration dependence was studied varying the box size containing one sink, in the present case we perform more general calculations where many mobile clusters are present in the calculation. In that case, it may not be necessary to choose “non-cubic” boxes (as opposed to “quasi-cubic” ones with  $L_x \simeq L_y \simeq L_z$  like, for example, a  $991 \times 997 \times 1009$  box would be, in lattice parameter  $a_0$  units).

## 3. Criteria for the convergence of CSS estimates

### *a. First criterion: compatibility between the box size and the number of clusters*

The previous condition is necessary but not sufficient to ensure correct estimating of the CSS. The box size should be carefully chosen so that there is at least one interacting pair along the shortest box dimension (linear densities of pairs times the shortest box dimension is greater than one). Adopting a slightly more probabilistic approach: assuming  $L_x \leq L_y \leq L_z$ , the probability of having more than two interacting species along one of the  $L_y L_z$  segments

of dimensionless length  $L_x$  [26] is

$$\begin{aligned}
P(N_t \geq 2) &= 1 - P(N_t = 0) - P(N_t = 1) \\
&= 1 - (1 - p)^{L_x} - L_x p (1 - p)^{L_x - 1} \\
&\simeq p^2 L_x^2,
\end{aligned} \tag{B1}$$

$$\tag{B2}$$

assuming a binomial distribution of A species along  $L_x$ . Here,  $p$  is the probability for one site to be occupied by an A particle:

$$p = C_A a_0^3 = \frac{N_A}{L_x L_y L_z}, \tag{B3}$$

is assumed to be small [27].

Noting that there is on average,

$$\frac{N_A}{L_y L_z} \tag{B4}$$

A-type particles along one  $L_x$  segment, one should then sum up the probability Eq.B2 over all the  $L_y L_z$  segments of length  $L_x$  (the probabilities for individual segment are assumed to be independent) for a criterion on having at least one  $L_x$  segment with two A-particles aligned. Note that, as stated before,  $A - A$  reactions are not accounted for, and the criteria we look for in fact concerns  $A - B$  interactions. But it turns out to be more simple to manipulate only one concentration  $C_A$ , and then extract a conservative criterion assuming  $C_A \leq C_B$ . Doing so, we end up with the following crudely approximated but conservative criterion

$$(p L_x)^2 L_y L_z \simeq 1. \tag{B5}$$

If, more realistically, one wishes to account for the minimum distance between species to be greater than twice the capture radius (defects are now placed on a grid now with spacing  $R$  instead of  $a_0$  and  $p$  is now  $C_A R^3$ ),

$$N_A^{\min} \gtrsim L_x \frac{a_0}{R}, \tag{B6}$$

with  $C_A \leq C_B$  and  $L_x \leq L_y \leq L_z$ , this gives the order of magnitude for the minimum number of species to place in the box to have a large proportion of  $A - B$  reactions. Note that this criterion should be conservative also regarding glide direction effects because it should be

even more easily met when glide directions are non-colinear to the boxes' directions as, in the case of  $\langle 111 \rangle$ -glide for example, interaction probabilities might be enhanced by the shift of linear trajectories after crossing a periodic boundary.

This criterion happens to be well validated if we consider the results of Fig. 12. On this graph are plotted the decimal logarithm of the ratio of CSS estimates from OKMC simulation over the analytical expression  $\kappa_{2D-0}^2$  [1]

$$2\pi\overline{R_{\text{eff}}}\frac{8}{-\ln(\pi^2/2(C_A + C_B)R^3)}C_B. \quad (\text{B7})$$

In these simulations (with the parameters  $E_A = E_B = 2$  eV,  $D_A = D_B$ ,  $R_A = R_B = 1$  nm), the analytical expression and simulation estimates of CSS should match at least within the uncertainty of the estimates (i.e. the  $\log_{10}$  of their ratio should reach 0 within the error bars on Fig. 12). This ratio is given as a function of  $\sqrt[3]{L_x L_y L_z}$  so a logarithm of the ratio far from zero denotes the inability of the simulation setup to reproduce correct sink strength values due to small box size effects which are notably sharp in the case of 1D-mobility simulations. On the caption of this figure is also displayed the minimum value

$$L_{\min} = \frac{1}{\sqrt{C_A R^3}} \quad (\text{B8})$$

of the box length corresponding to each concentration  $C_A = C_B$  obtained applying preceding criterion Eq. B5 but for a fixed concentration (for this criterion  $L_x \simeq L_y \simeq L_z$  is assumed). We see that this simplistic criterion catches reasonably well the order of magnitude of the box dimension for onset of convergence: below these values the convergence is not reached regarding standard deviations of the estimates.

*b. Second criterion: relation between number of clusters and minimal number of reactions*

The first criterion ensured us that, for a given concentration, the box will be large enough so that all A-clusters have at least one B-type partner for a potential reaction. Another criterion is needed on the extend of the reactions sampling so that most of this type of reactions have a chance to occur. This criterion on the convergence of the CSS estimates is that starting from one initial random configuration of mobiles, the sampling of reactions should be extended enough to have at least as much absorptions recorded as the total number of mobiles. This is because absorption rates should reflects all contributions to the reaction

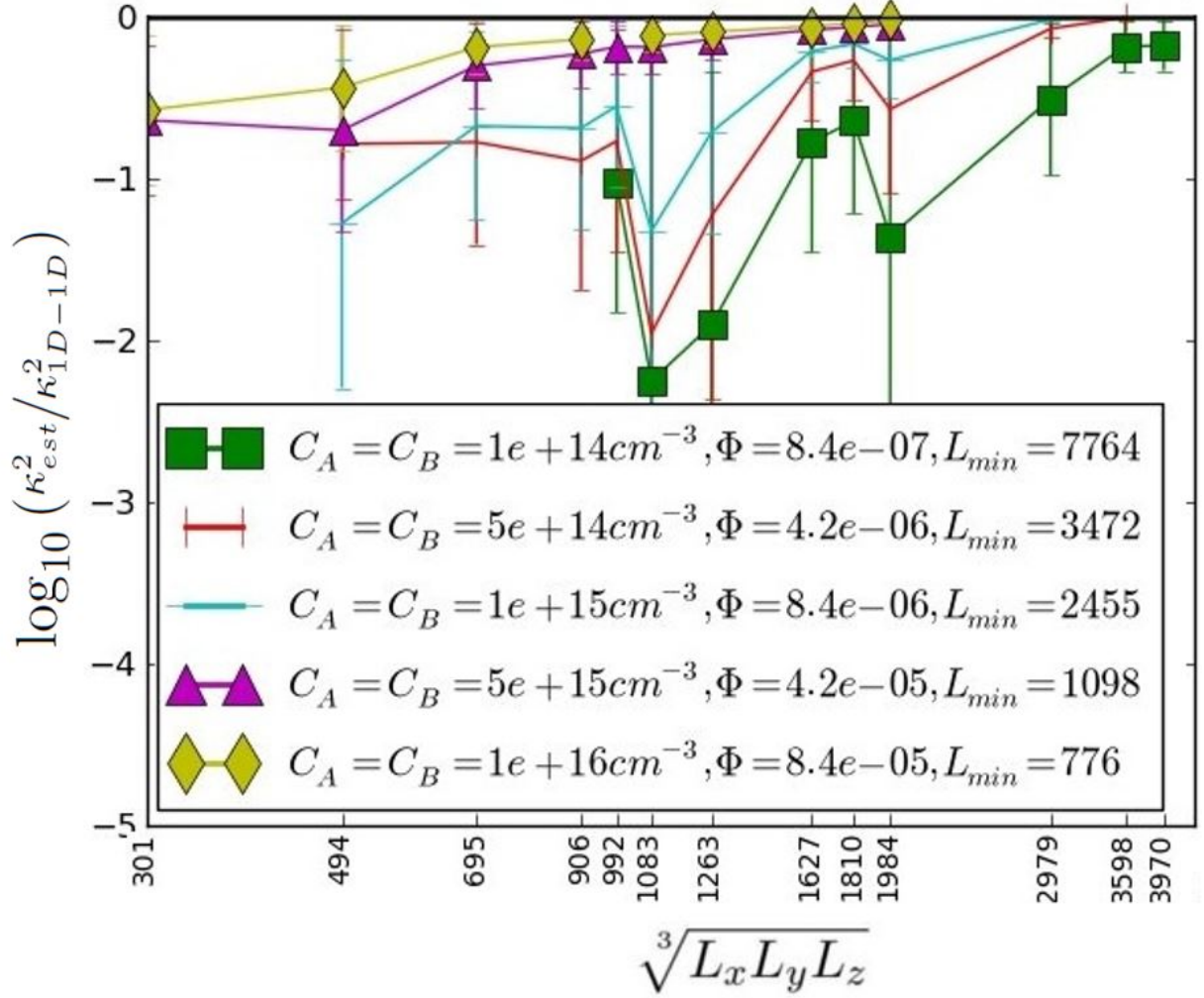


Figure 12. Decimal logarithm of the ratio of estimated CSS over the analytical value ( $\log_{10}(\kappa_{est}^2/\kappa_{1D-1D}^2)$ ) as a function of  $\sqrt[3]{L_x L_y L_z}$  for various  $(C_A, R)$  couples. Points of a given curve all correspond to same computation times. It is clear that significant convergence is reached only when the box size reaches approximately the  $L_{min}$  criterion.

probabilities: on one hand reactions occurring by very fast 1D interactions of defects which are very close but rare according to the random distribution of initial distances and, on the other hand, contributions from the vast majority of slow (due to the inefficient 1D-sampling of space) non-colinear 1D-1D reactions. Stopping the run before having significant chances that all mobiles had at least one interaction, and restarting it with another initial random configuration of defect would result in sampling only the fast reactions and thus over-estimating the CSS. A direct consequence is that it limits the use of naive parallelization [28] for the longest calculation: each run must be continued until most defects of both type

have reacted. This point is also very important and if it is overlooked it can be a major source of inaccuracy of CSS estimations: the CSS may vary by several orders of magnitudes going from fast components to its slowest ones.

*c. Third criterion: averaging estimates over several runs*

Applying the second criterion with a given initial configuration, one produces a single estimate of CSS by averaging the reaction time for a number of reaction greater than the total number of mobiles. Now, from the statistical point of view, one should estimate the average error related to estimates. As a consequence, one should sample several tens of initial configurations, average the CSS estimates and judge whether the sampling is sufficient to have a low standard deviation to mean ratio.

### **Appendix C: Temperature and lattice dependent semi-analytical formula**

In the semi-analytical expression of CSS, the transition function between well defined analytical CSS were fitted on OKMC calculation for a given lattice type, a given first nearest neighbor distance and at a given temperature. To generalize it, we may first note that the temperature only plays a role in the mean-free path before rotation  $\ell$  as the formula is directly parameterized on diffusion coefficients. It may then be adapted to depend on the couple  $(\ln(\ell_A), \ln(\ell_B))$ , with

$$\ln(\ell) = \frac{E}{2k_B T} + \ln d_j, \quad (\text{C1})$$

instead of rotation energies  $(E_A, E_B)$ . Also as  $1DR - 0$  type CSS limiting cases are not explicitly accounted, only the sigmoid transition functions must be adapted:

$$\sigma'(\ell, \lambda, \varepsilon, T) = \frac{1}{1 + \exp \left[ -2\lambda k_B T_0 \left( \ln(\ell) - \ln(d_j) - \frac{\varepsilon}{2k_B T} \right) \right]}, \quad (\text{C2})$$

which ensures  $\sigma'(\ell, \lambda, \varepsilon, T_0) = \sigma(E, \lambda, \varepsilon)$ . In fact this formulation is useful only when adapting to both a different temperature and a different lattice (reflected by jump distance  $d_j$ ).

When only adapting to a different temperature, the transformation may be reduced to substituting  $E$ ,  $\varepsilon$  and  $\lambda$  to  $E/T$ ,  $\varepsilon/T$ ,  $\lambda/T_0$  respectively in the original expressions of the sigmoids. The discrepancies related to the absence of  $1DR - 0$  terms in the fit could possibly be enhanced when applying to other temperatures, so the quality of the adapted fit at  $T = 300\text{ K}$  and  $T = 800\text{ K}$  was studied. The isosurfaces of the ratios  $\kappa_{\text{eff}}^2/\kappa_{\text{fit}}^2$  are shown on Fig. 13. The situation is almost opposite in the two cases. For the low temperature, the discrepancy gets higher but in an even more restricted zone than at the reference temperature, so the overall accuracy is not significantly changed (about 18 %). For the higher temperature, the maximum discrepancy is lower than for the reference, but it is more widespread over the parameter volume, and the location of the maximum discrepancy (about 2) is different. This also leads to a global accuracy of the same order as for the initial fitting temperature (about 23 %). This also suggest to use temperature dependent terms in the transition functions for applications requiring much higher levels of accuracy.

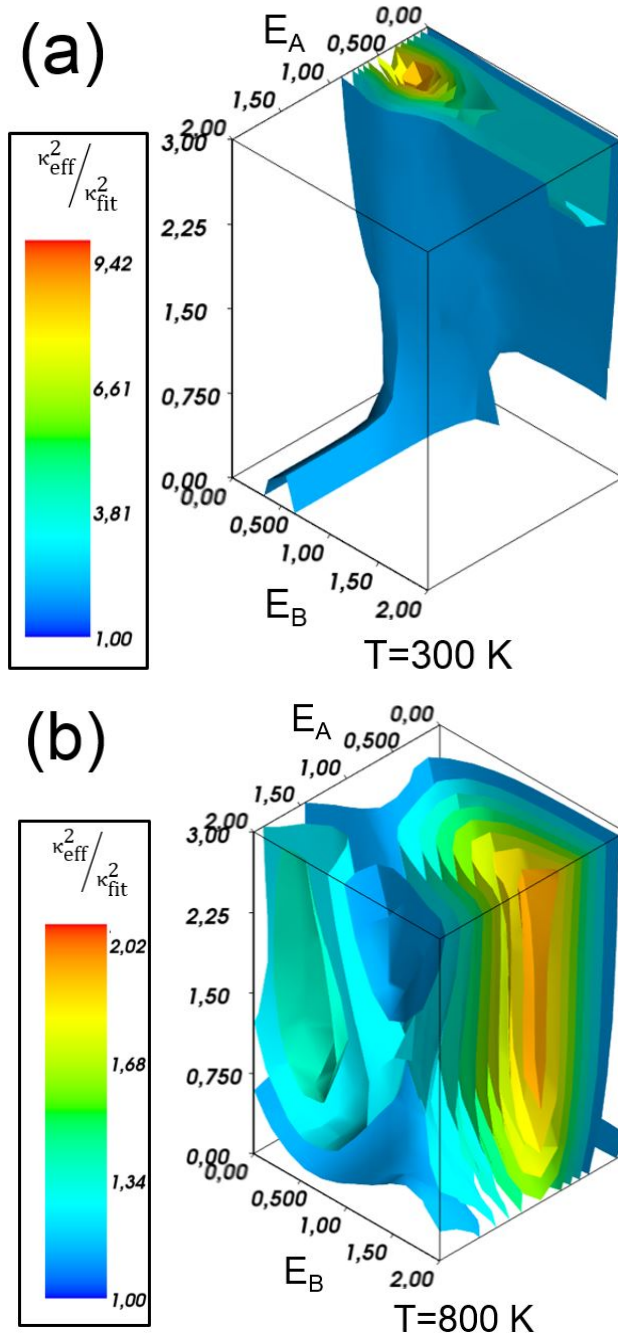


Figure 13. Isosurfaces of the ratios  $\kappa_{\text{eff}}^2/\kappa_{\text{fit}}^2$ . (a)  $T = 300\text{ K}$ , (b)  $T = 800\text{ K}$ , and  $C_A = C_B = 5 \times 10^{16}\text{cm}^{-3}$ ,  $R_A = R_B = 1\text{ nm}$  in both cases. The vertical axis represents  $\Delta$ .